PHILOSOPHICAL TRANSACTIONS OF THE ROYAL SOCIETY A MATHEMATICAL, PHYSICAL & ENGINEERING SCIENCES

A Two-Dimensional Numerical Sea Model

N. S. Heaps

Phil. Trans. R. Soc. Lond. A 1969 **265**, 93-137
doi: 10.1098/rsta.1969.0041

A TWO-DIMENSIONAL NUMERICAL SEA MODEL

By N. S. HEAPS

The University of Liverpool Tidal Institute and Observatory, Birkenhead, Cheshire*

(*Communicated by J. Proudman, F.R.S.—Received* 22 *November* 1968—
Revised 20 *January* 1969)

CONTENTS

The model has, in the first place, been developed for the detailed investigation of various types of North Sea storm surge, particularly the external surge. As in some earlier investigations the linearized hydrodynamical equations are solved numerically by using a finite-difference grid and a step-by-step procedure in time. However, a special feature of the present approach is that, within the basic grid system, it is possible to choose a general form of sea boundary: the computations are then carried out accordingly, on a digital computer, using an Algol program. In this sense the aim has been to develop a numerical tool of fairly wide application for the study of surge and tidal phenomena in adjacent seas.

For the North Sea, surges experienced at several ports around the shores of the Sea have been compared with those derived numerically. Also, contour lines of sea-level disturbance have been drawn showing patterns of surge development. Perhaps for the first time, the continental shelf sea surrounding the British Isles has been treated as a single dynamical unit, and the influence of flow through the Strait of Dover on surge levels in the North Sea has been studied.

The work has laid out guide lines for future research involving the application of numerical models to problems of storm surges and tides in British waters. A first step has been taken towards the establishment of a surge forecasting system for the east coast of England based on dynamical principles.

1. Introduction

During recent years, numerical methods have been used increasingly to solve the differential equations which govern the motion of the sea under the action of tidal and meteorological forces. As a result, tides and storm surges have been computed for a wide range of natural sea basins (Hansen 1956, 1962, 1966; Platzman 1958, 1963, 1965; Fischer 1959; Uusitalo 1960; Lauwerier 1962; Lauwerier & Damsté 1963; Miyazaki, Ueno & Unoki 1961, 1962; Ueno 1964;

* Now renamed The Institute of Coastal Oceanography and Tides.

Vol. 265. A. 1160. (Price £1 3*s*.; U.S. $3.00) 12 [Published 30 October 1969

Miyazaki 1965; Jelesnianski 1965, 1966; Laska 1966; Leendertse 1967). An important concept in the work has been the formulation of numerical sea models, representing, in numerical terms, the geometrical and dynamical properties of the natural basins. Within the framework of such a model, the hydrodynamical equations, expressed in terms of finite differences, have formed the basis of an iterative procedure by which tides and surges have been built up numerically at a series of time levels, stepping forward from some given initial state of displacement and motion. The mathematical fundamentals of this procedure have been elucidated by Richtmyer (1957) in his account of difference methods for initial-value problems. Discussions on the application of the procedure to tidal and storm surge problems have been given by Harris & Jelesnianski (1964) and earlier by Welander (1961).

Employing the numerical approach mentioned above, the present work has had four main objects:

(i) To design a model for the calculation of storm surges in a sea of general boundary configuration. The essential idea has been to express the geometry of the land and open-sea boundaries of the model in terms of numerical parameters which may be varied, within the same computational system, to give sea basins of different shapes and sizes. A model with this property could be regarded as a research tool for the investigation of surge phenomena, complementing analytical methods used, for example, by Dantzig & Lauwerier (1960 *a*, *b*), Lauwerier (1960 *a*, *b*, *c*, 1961 *a*, *b*) and Heaps (1965)

(ii) To reproduce numerically storm surges of various types experienced in the North Sea and to gain an insight into the mechanics of their generation and propagation. In particular, an important aim has been to obtain an understanding of the origin of the so-called 'external' surge which, from observation, appears to enter the North Sea through its northern opening and then travel southwards as a single wave, affecting sea levels along the east coast of the British Isles (Corkan 1948).

(iii) To lay the foundations of a possible surge-forecasting system for ports on the east coast of England. Such a system would be one based primarily on dynamical principles, rather than one dependent on purely empirical formulae derived from the statistical analysis of past surges (Rossiter 1959).

(iv) To initiate a long-term programme of research into the application of numerical techniques to determine tides and surges in seas and oceans.

It will be shown in later sections of this paper that these aims have, to a satisfactory extent, been realized. A numerical sea model has been formulated in which the dynamical equations for storm surges, taken in linearized vertically-integrated form, are solved by using a difference scheme similar to that considered by Lauwerier (1962). The scheme is characterized by the replacement of the time derivatives in the equations by a combination of forward and backward time differences, and the space derivatives by averaged central space differences. Sea surface elevations and depth-mean currents are evaluated at the intersections of a grid formed by parallels of latitude and lines of longitude. The coastal and open-sea boundaries of the model are traced out on the grid, following, as closely as possible, the boundaries of the natural sea basin under consideration. A fairly arbitrary form of model boundary may be taken in this way, thus allowing for the representation of a variety of sea basins with differing geometries.

The system of numerical model calculations has been programmed in ALGOL for running on the English Electric KDF 9 electronic digital computer. The program makes possible the computation of surges generated from a state of rest by wind fields acting respectively over arbitrarily

selected subareas of the model sea. As input data, wind velocity may be specified at regular intervals over a set of such areas, simulating actual wind conditions over the natural sea; the resulting output then yields surge elevations which may be compared with elevations deduced from sea-level observations after removal of the tides and the effects of changes in barometric pressure.

Three particular models, of successively increasing size, have been considered for the calculation of North Sea surges. The first covers the North Sea area and the shelf sea areas to the north and west of Scotland, the Strait of Dover being closed. The second takes account of flow through the Strait and extends over most of the northwestern European shelf, representing the North Sea and the other sea regions surrounding the British Isles. The third consists of the latter model extended beyond the shelf edge to take in an area of oceanic water to the northwest of Scotland. The models have been used to compute the wind-induced disturbances of sea level corresponding to three different North Sea surges: an external surge (13 to 15 September 1956), a surge generated in the southern part of the North Sea (24 to 26 February 1958), and the notorious 'Hamburg' surge (15 to 17 February 1962). In this way, it has been possible to reproduce to a first approximation the actual surge heights (corrected for the effects of barometric pressure) experienced at various ports distributed around the North Sea coast. Comparison of results, as between models, has indicated the extent to which flow through the Dover Strait influences surge levels. The external surge has received special attention: it has been shown that the disturbance was mainly generated by wind fields acting over an area of shelf sea lying to the north of Scotland, the time sequence of the fields being of importance to the development of the surge.

The significance of the present work lies in the formulation of a numerical sea model of fairly general application, and the use of the model to investigate North Sea surges of different types—demonstrating its potentialities for surge forecasting. Perhaps for the first time, the waters surrounding the British Isles have been considered together in one dynamical system.

2. Basic differential equations

The dynamical equations for storm surges, linearized and integrated with respect to the depth, have been given by Proudman (1954). Taking latitude and east-longitude as space coordinates the equations are

$$\frac{1}{a\cos\phi}\left\{\frac{\partial}{\partial\phi}(U\cos\phi)+\frac{\partial V}{\partial\chi}\right\}+\frac{\partial\zeta}{\partial t}=0, \tag{1}$$

$$\frac{\partial U}{\partial t}+2\omega\sin\phi V=-\frac{gh}{a}\frac{\partial\zeta}{\partial\phi}-\frac{h}{\rho a}\frac{\partial p_a}{\partial\phi}+\frac{1}{\rho}(F_S-F_B), \tag{2}$$

$$\frac{\partial V}{\partial t}-2\omega\sin\phi U=-\frac{gh}{a\cos\phi}\frac{\partial\zeta}{\partial\chi}-\frac{h}{\rho a\cos\phi}\frac{\partial p_a}{\partial\chi}+\frac{1}{\rho}(G_S-G_B), \tag{3}$$

where the notation is as follows:

ϕ, χ	latitude and east-longitude, respectively
t	the time
ζ	the elevation of the sea surface
$U, V,$	the components of the total stream
F_S, G_S	the components of the friction of the wind on the sea surface
F_B, G_B	the components of the friction of the water on the sea bottom
p_a	the atmospheric pressure on the sea

PHILOSOPHICAL TRANSACTIONS OF THE ROYAL SOCIETY A MATHEMATICAL, PHYSICAL & ENGINEERING SCIENCES

h	the undisturbed depth of the water
ρ	the density of the water, assumed uniform
a	the mean radius of the Earth
g	the acceleration of the Earth's gravity
ω	the angular speed of the Earth's rotation

The component directions are those of increasing ϕ, χ respectively, i.e. to the north and to the east. By definition,

$$U = \int_0^h u\,dz, \quad V = \int_0^h v\,dz, \tag{4}$$

where u, v denote the components of horizontal current at depth z below the undisturbed sea-surface.

On the basis of work by Bowden (1953, 1956) it is assumed that

$$F_B = \lambda\rho U, \quad G_B = \lambda\rho V \quad (\lambda = \kappa/h), \tag{5}$$

taking $\kappa = 0.24$ cm/s, the value estimated by Weenink (1958) for the southern North Sea.

Taking $a = 6.37 \times 10^3$ km, $g = 32.2$ ft/s^2, $\rho = 1.025$ g/cm^3 and, for practical convenience, measuring ϕ and χ in degrees, t in hours, h in fathoms, ζ in feet, depth-mean currents U/h and V/h in feet per second, stresses F_S, G_S in dynes per square centimetre, p_a in millibars, and both λ and ω in reciprocal hours, the equations (1) to (3) reduce to

$$\frac{\partial\zeta}{\partial t} = -\frac{\alpha}{\cos\phi}\left\{\frac{\partial}{\partial\phi}(U\cos\phi) + \frac{\partial V}{\partial\chi}\right\}, \tag{6}$$

$$\frac{\partial U}{\partial t} = -\lambda U - 2\omega\sin\phi V - \beta h\frac{\partial\zeta}{\partial\phi} + \gamma P, \tag{7}$$

$$\frac{\partial V}{\partial t} = -\lambda V + 2\omega\sin\phi U - \frac{\beta h}{\cos\phi}\frac{\partial\zeta}{\partial\chi} + \gamma Q, \tag{8}$$

where

$$P = F_S - \delta h\frac{\partial p_a}{\partial\phi}, \quad Q = G_S - \frac{\delta h}{\cos\phi}\frac{\partial p_a}{\partial\chi} \tag{9}$$

and $\alpha = 0.05922$, $\beta = 0.31780$, $\gamma = 0.63008$, $\delta = 0.01645$.

The equations (6) to (9) are used in the present work as a basis for the determination of *wind-generated* surges, whence $\partial p_a/\partial\phi = \partial p_a/\partial\chi = 0$ in (9), giving

$$P = F_S, \quad Q = G_S. \tag{10}$$

Thus, P and Q may be identified with the wind stress components directed to the north and to the east, respectively, at any location (ϕ, χ).

The problem to be considered is that of solving equations (6), (7), (8) to find the variations of ζ, U, V over a sea area, given the changing distributions of P and Q over the sea surface. The primary aim is to determine the surge elevation ζ. It is assumed that surges are generated from an initial state of rest, so that $\zeta = U = V = 0$ everywhere at $t = 0$. Certain conditions on ζ, U, V have to be satisfied, for all $t \geqslant 0$, along the lateral boundaries of the sea area. Thus, zero normal flow across a coast line requires

$$U\cos\psi + V\sin\psi = 0 \tag{11}$$

at coastal points, where ψ denotes the inclination of the normal to the northerly direction. Along an open boundary, ζ may be specified as a function of position and time, representing

surge propagation across the boundary. Alternatively, if the sea basin is relatively shallow and its open boundary is contiguous with a deep ocean, as is true of the basins considered in the present work, then the condition

$$\zeta = 0 \quad (\text{for all } t \geqslant 0) \tag{12}$$

along the boundary, may be reasonably assumed (Veltkamp 1954; Groen & Groves 1962).

The hydrodynamical equations are considered in linearized form in order that solutions, giving responses of sea level to a number of standard wind fields, may be superimposed to obtain responses to more general fields; this is the *influence* method for the determination of surge heights described by Welander (1961). However, by reason of their linearity, the equations take no account of the nonlinear coupling between tides and surges, important in shallow coastal regions and estuaries.

The assumption of vertically-integrated equations as the starting-point for this paper follows the procedure of earlier numerical-model investigations. Integration with respect to the depth eliminates dependence on the depth coordinate, thereby introducing a simplification. Solutions then determine elevations and total streams, but give no information concerning the vertical structure of current.

3. The finite-difference grid

The type of finite-difference grid used in the solution of the basic differential equations is shown in figure 1. The grid lines consist of parallels of latitude (horizontals) spaced at intervals of $\Delta\phi$ degrees, and lines of longitude (verticals) at intervals of $\Delta\chi$ degrees. Grid points are of two kinds: 'elevation' points (denoted by circles) at each of which ζ is evaluated, and 'stream' points (denoted by crosses) at each of which U and V are evaluated. By design, the array of points is bounded by elevation points to the north and to the west, and by stream points to the south and to the east.

In general, the number of grid points along each parallel of latitude is denoted by n and the number of parallels by $2p$. Thus, for the array shown in figure 1, $n = 14$ and $p = 9$. For a fixed mesh size $(\Delta\phi, \Delta\chi)$ the choice of n and p determines the overall dimensions of the grid and hence the area it covers. Both elevation and stream points are numbered $i = 1, 2, 3, \ldots, np$ moving southwards through the grid system counting from west to east along alternate parallels (figure 2). The latitudes of successive parallels are denoted by ϕ_j $(j = 1, 2, 3, \ldots, 2p)$ where $\phi = \phi_1$ gives the northern limit of the grid. Then, letting ζ_i denote the value of ζ at the elevation point i and U_i, V_i the values of U, V at the stream point i, we have

$$\zeta = \zeta_i, \quad \phi = \phi_{2k-1} \text{ at elevation point } i, \tag{13.1}$$

$$U = U_i, \quad V = V_i, \quad \phi = \phi_{2k} \text{ at stream point } i, \tag{13.2}$$

where

$$k = 1 + \text{int}\left(\frac{i-1}{n}\right) \tag{13.3}$$

for $i = 1(1)np$, int indicating that the integral part is taken. The use of a single suffix notation to define array values facilitates the programming of the numerical work.

The grid system, described above, is chosen so that it completely covers the area of the natural sea basin under consideration. A sea model, representing the natural basin, is then marked out on the grid-lines. The coastal boundaries of the model are formed by line-segments connecting stream points; the open sea boundaries by line-segments connecting elevation points. This

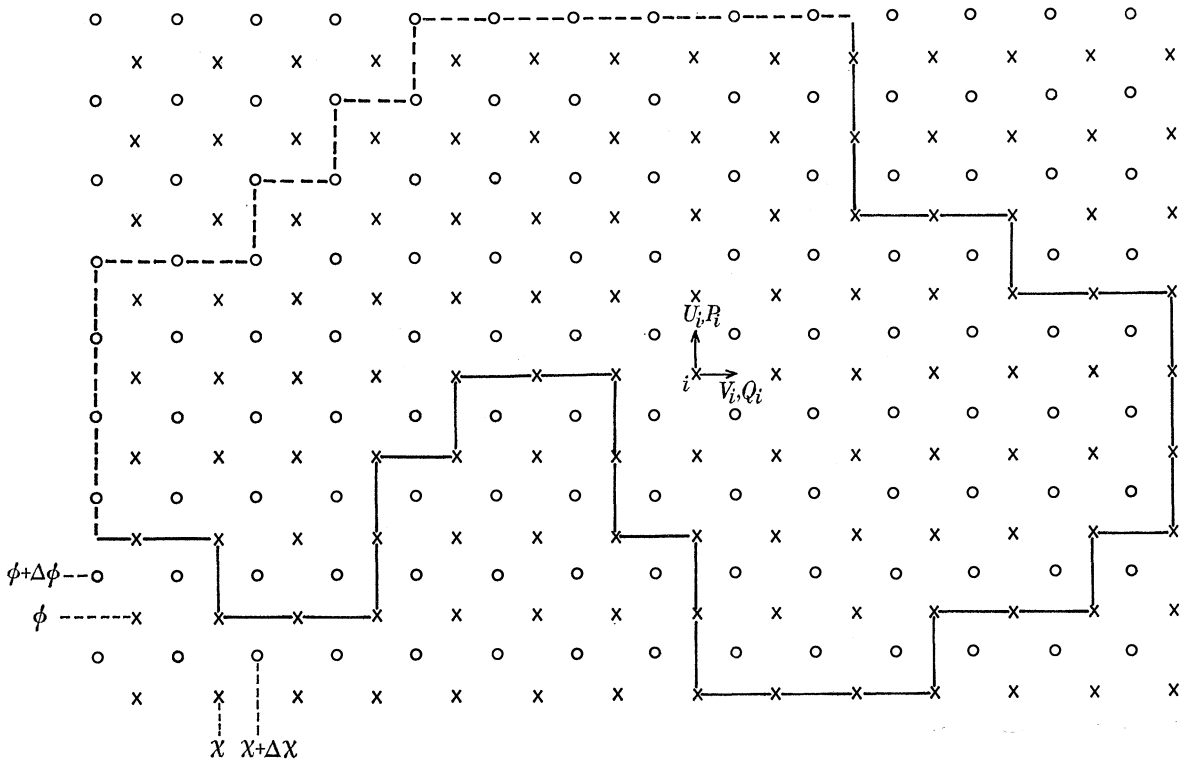

FIGURE 1. Diagram indicating the type of finite-difference grid used in the numerical solution of the hydrodynamical equations. Horizontals represent parallels of latitude, and verticals lines of longitude. The boundaries of a sea model are shown marked on the grid; ○, elevation point; ×, stream point; ---○--, open-sea boundary; —×–, coastal boundary.

TABLE 1. THE ARRAY OF INTEGER LABELS DEFINING THE BOUNDARY OF THE SEA MODEL SHOWN IN FIGURE 1

1	1	1	1	2	2	2	2	2	2	1	1	1	1	
4	4	4	4	22	22	22	22	22	8	4	4	4	4	
1	1	1	2	2	3	3	3	3	3	1	1	1	1	
4	4	4	22	22	22	22	22	22	6	4	4	4	4	
1	1	2	2	3	3	3	3	3	3	1	1	1	1	
4	4	22	22	22	22	22	22	22	18	13	5	4	4	
2	2	2	3	3	3	3	3	3	3	3	3	1	1	
22	22	22	22	22	22	22	22	22	22	22	18	13	5	
2	3	3	3	3	3	3	3	3	3	3	3	3	3	
22	22	22	22	19	12	20	22	22	22	22	22	22	6	
2	3	3	3	3	1	1	3	3	3	3	3	3	3	
22	22	22	19	5	4	7	22	22	22	22	22	22	6	
2	3	3	3	1	1	1	3	3	3	3	3	3	3	
14	20	22	6	4	4	5	20	22	22	22	22	19	5	
1	1	3	3	1	1	1	1	3	3	3	3	3	1	
4	5	12	5	4	4	4	7	22	22	19	12	5	4	
1	1	1	1	1	1	1	1	3	3	3	1	1	1	
4	4	4	4	4	4	4	5	12	12	5	4	4	4	

method of boundary construction is illustrated diagrammatically in figure 1 and its application in the design of three North Sea models is demonstrated in figures 8 to 10. The smaller the mesh size, the more closely is it possible to represent the boundary of the natural sea by the step-like boundary configuration of the model.

An elevation point i is located either outside the model sea, on one of its open boundaries, or within the sea.

A stream point i is located either outside the sea, on one of its coastal boundaries, or within the sea. When positioned on a coastal boundary it may either be a corner point at the apex of a 90° sector of sea—any one of the four cases in figure 3 (*a*); or it may lie on a longitudinal section of boundary, six cases being admitted as shown respectively in figures 3 *b* to *g*; or it may lie on a latitudinal section of boundary, again six cases being admitted as shown respectively in figures 3 *h* to *m*; or it may be a corner point at the apex of a 270° sector of sea, four cases being admitted as shown repectively in figures 3 *n* to *q*.

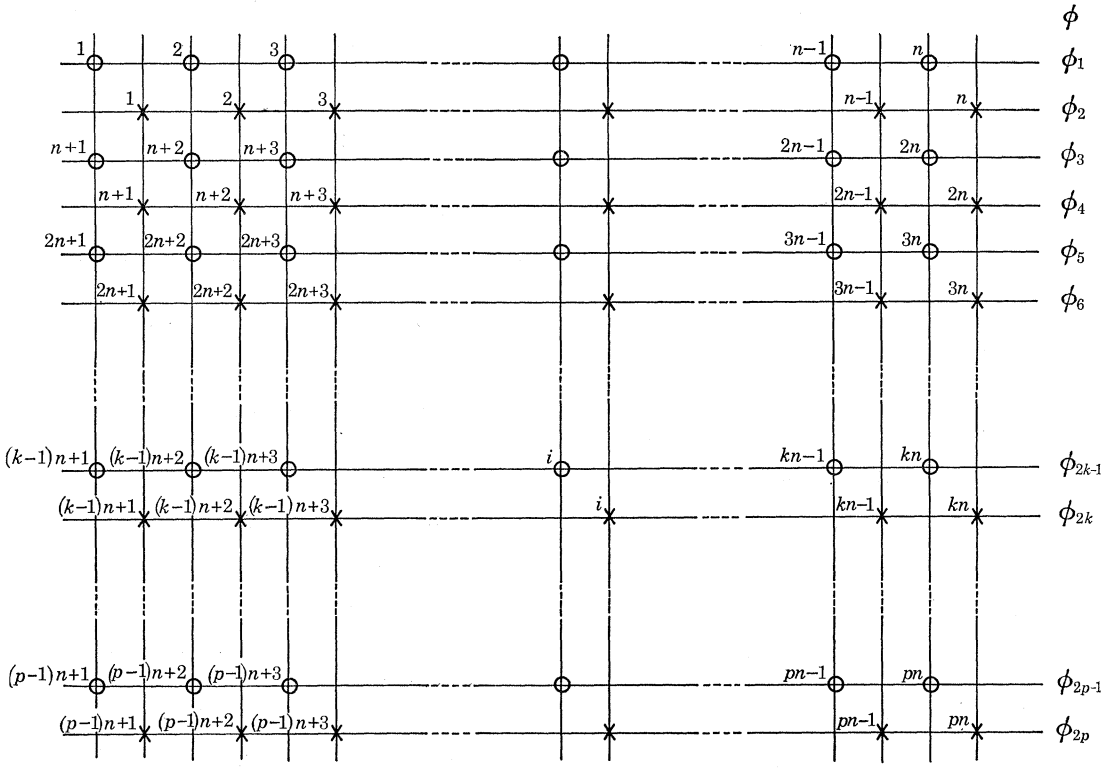

FIGURE 2. Numbering system for the grid points.

It follows that there are 22 different types of grid-point location, denoted respectively by integers 1 to 22 as indicated below:

Elevation point

outside the model boundary		1
on the boundary		2
within the boundary		3

Stream point

outside the model boundary		4
at a 90° corner of the boundary	figure 3 *a*	5
on a longitudinal section of the boundary	figure 3 *b*	6

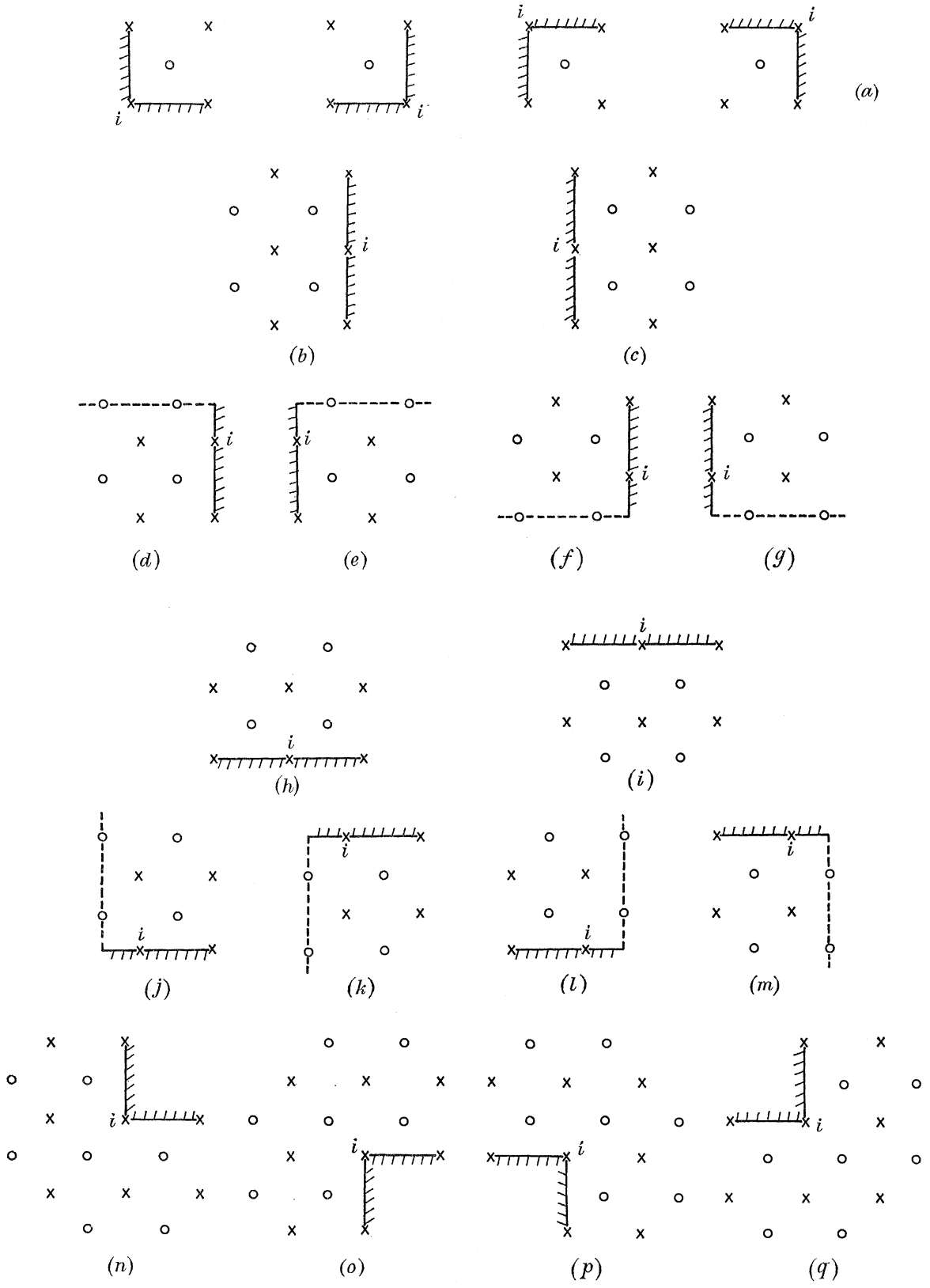

FIGURE 3. Elemental grid-point arrays, showing admissible locations of a stream point i on a coastal boundary of the model sea; ------, open-sea boundary; sea / land, coastal boundary.

PHILOSOPHICAL TRANSACTIONS OF THE ROYAL SOCIETY A MATHEMATICAL, PHYSICAL & ENGINEERING SCIENCES

on a longitudinal section of the boudary	figure 3*c*	7
	figure 3*d*	8
	figure 3*e*	9
	figure 3*f*	10
	figure 3*g*	11
on a latitudinal section of the boundary	figure 3*h*	12
	figure 3*i*	13
	figure 3*j*	14
	figure 3*k*	15
	figure 3*l*	16
	figure 3*m*	17
at a 270° corner of the boundary	figure 3*n*	18
	figure 3*o*	19
	figure 3*p*	20
	figure 3*q*	21
within the boundary		22

Labelling each grid point with the integer appropriate to its location, yields an array of integers defining, for the purposes of the numerical calculations, the boundary configuration of the model sea. (By way of example, table 1 gives the array corresponding to the model marked out in figure 1.)

Values of ζ, U, V at grid points lying outside the sea are purely fictitious and have no physical significance; they are allocated to control the output format of the computed elevations and streams associated with the grid points of the sea area.

The depth h, the frictional parameter λ, and the components of wind stress P, Q are defined at every stream point lying within or on the model boundary. Their respective values at stream point i are denoted by h_i, λ_i, P_i, Q_i so that we have:

$$h = h_i, \quad \lambda = \lambda_i\,(=\kappa/h_i), \quad P = P_i, \quad Q = Q_i, \tag{14}$$

at each stream point i of the model

4. Difference equations

The basic differential equations (6), (7), (8) are now replaced by finite-difference equations relating ζ_i, U_i, V_i at a time $t+\tau$ to the values of these variables at a preceding time t, τ being an elementary time-step. The difference scheme, using forward and backward differences in time and central differences in space, is similar to that employed by Lauwerier (1962) and Lauwerier & Damsté (1963); essentially, it may be regarded as a development of a scheme due to Fischer (1959). However, as will become apparent subsequently, more detailed consideration is given to boundary conditions than in this earlier work.

At an elevation point i lying within the model sea (a grid point with integer label 3, as defined in § 3) the equation of continuity (6) is replaced by

$$\frac{\zeta_i(t+\tau)-\zeta_i(t)}{\tau} = -\frac{\alpha}{\cos\phi_{2k-1}}\left\{\frac{B_i(t+\tau)}{2\Delta\phi}+\frac{C_i(t+\tau)}{2\Delta\chi}\right\}, \tag{15}$$

where (figure 4 *a*):

$$\left.\begin{aligned} B_i &= \tfrac{1}{2}(U_{i-n}\cos\phi_{2k-2} - U_i\cos\phi_{2k} + U_{i-n-1}\cos\phi_{2k-2} - U_{i-1}\cos\phi_{2k}),\\ C_i &= \tfrac{1}{2}(V_i - V_{i-1} + V_{i-n} - V_{i-n-1}). \end{aligned}\right\} \tag{16}$$

At a stream point i within the sea (a grid point with integer label 22) the equations of motion (7), (8) are replaced by

$$\frac{U_i(t+\tau) - U_i(t)}{\tau} = -\lambda_i U_i(t) - 2\omega\sin\phi_{2k}V_i(t) - \beta h_i\frac{D_i(t)}{2\Delta\phi} + \gamma P_i(t), \tag{17}$$

$$\frac{V_i(t+\tau) - V_i(t)}{\tau} = -\lambda_i V_i(t) + 2\omega\sin\phi_{2k}U_i(t) - \frac{\beta h_i}{\cos\phi_{2k}}\frac{E_i(t)}{2\Delta\chi} + \gamma Q_i(t), \tag{18}$$

where (figure 4 *b*):

$$\left.\begin{aligned} D_i &= \tfrac{1}{2}(\zeta_i - \zeta_{i+n} + \zeta_{i+1} - \zeta_{i+n+1}),\\ E_i &= \tfrac{1}{2}(\zeta_{i+1} - \zeta_i + \zeta_{i+n+1} - \zeta_{i+n}). \end{aligned}\right\} \tag{19}$$

A rearrangement of (15), (17) and (18) yields

$$U_i(t+\tau) = (1-\tau\lambda_i)\,U_i(t) - 2\tau\omega\sin\phi_{2k}V_i(t) - \frac{\tau\beta h_i D_i(t)}{2\Delta\phi} + \tau\gamma P_i(t), \tag{20.1}$$

$$V_i(t+\tau) = (1-\tau\lambda_i)\,V_i(t) + 2\tau\omega\sin\phi_{2k}U_i(t) - \frac{\tau\beta h_i E_i(t)}{2\cos\phi_{2k}\Delta\chi} + \tau\gamma Q_i(t), \tag{20.2}$$

$$\zeta_i(t+\tau) = \zeta_i(t) - \frac{\alpha\tau}{\cos\phi_{2k-1}}\left\{\frac{B_i(t+\tau)}{2\Delta\phi} + \frac{C_i(t+\tau)}{2\Delta\chi}\right\}, \tag{20.3}$$

which are the basic difference equations of the present work.

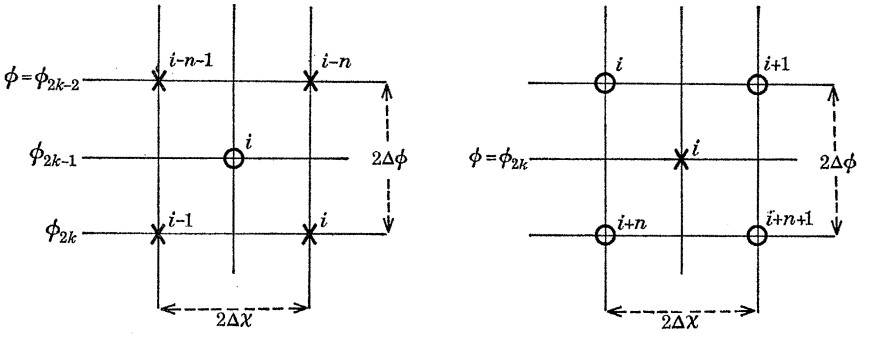

FIGURE 4. (*a*) Stream points used in the formulation of space differences B_i, C_i at an elevation point i within the model sea. (*b*) Elevation points used in the formulation of space differences D_i, E_i at a stream point i within the model sea.

At stream points i on the coastal boundaries of the model sea (points with integer labels 5 to 21), representation of the coastal boundary condition (11) leads to modified forms for D_i, E_i. Thus, at a corner point i lying at the apex of a 90° sector of sea (figure 3 *a*), we take

$$U_i = V_i = 0 \tag{21.1}$$

for all time, so that, from (20.1) and (20.2),

$$D_i = \frac{\gamma P_i}{\beta h_i/2\Delta\phi}, \quad E_i = \frac{\gamma Q_i}{\beta h_i/2\cos\phi_{2k}\Delta\chi}. \tag{21.2}$$

Further, at a stream point i on a longitudinal section of boundary (figures 3 b to g) the coastal condition is expressed by

$$V_i = 0 \tag{22.1}$$

and therefore, from (20.1) and (20.2),

$$U_i(t+\tau) = (1-\tau\lambda_i)\, U_i(t) - \frac{\tau\beta h_i D_i(t)}{2\Delta\phi} + \tau\gamma P_i(t), \tag{22.2}$$

$$E_i = \frac{2\omega \sin\phi_{2k} U_i + \gamma Q_i}{\beta h_i / 2\cos\phi_{2k}\Delta\chi}. \tag{22.3}$$

Forms taken for D_i in (22.2) may be grouped as follows:

Stream point i on a longitudinal boundary,

with land to the east (figure 3 b):

$$D_i = \tfrac{1}{16}\{18(\zeta_i - \zeta_{i+n}) - 2(\zeta_{i-1} - \zeta_{i+n-1}) + 3(E_{i-n} - E_{i+n})\}, \tag{22.4}$$

with land to the west (figure 3 c):

$$D_i = \tfrac{1}{16}\{18(\zeta_{i+1} - \zeta_{i+n+1}) - 2(\zeta_{i+2} - \zeta_{i+n+2}) - 3(E_{i-n} - E_{i+n})\}, \tag{22.5}$$

with land to the east and an open boundary to the north (figure 3 d):

$$D_i = \tfrac{1}{8}\{9(\zeta_i - \zeta_{i+n}) - (\zeta_{i-1} - \zeta_{i+n-1}) + 3(E_i - E_{i+n})\}, \tag{22.6}$$

with land to the west and an open boundary to the north (figure 3 e):

$$D_i = \tfrac{1}{8}\{9(\zeta_{i+1} - \zeta_{i+n+1}) - (\zeta_{i+2} - \zeta_{i+n+2}) - 3(E_i - E_{i+n})\}, \tag{22.7}$$

with land to the east and an open boundary to the south (figure 3 f):

$$D_i = \tfrac{1}{8}\{9(\zeta_i - \zeta_{i+n}) - (\zeta_{i-1} - \zeta_{i+n-1}) - 3(E_i - E_{i-n})\}, \tag{22.8}$$

with land to the west and an open boundary to the south (figure 3 g):

$$D_i = \tfrac{1}{8}\{9(\zeta_{i+1} - \zeta_{i+n+1}) - (\zeta_{i+2} - \zeta_{i+n+2}) + 3(E_i - E_{i-n})\}. \tag{22.9}$$

To derive D_i given by (22.4), referring to figure 5 a, we write

$$\zeta_{i+1} - \zeta_i = \tfrac{1}{2}(E_i + E_{i-n}), \quad \zeta_{i+n+1} - \zeta_{i+n} = \tfrac{1}{2}(E_i + E_{i+n}),$$

whence

$$\zeta_{i+1} - \zeta_{i+n+1} = \zeta_i - \zeta_{i+n} + \tfrac{1}{2}(E_{i-n} - E_{i+n}). \tag{23}$$

Then, a three-point Lagrange interpolation between $\zeta_{i+1} - \zeta_{i+n+1}$, $\zeta_i - \zeta_{i+n}$ and $\zeta_{i-1} - \zeta_{i+n-1}$, making evaluation on the longitudinal coastal boundary through the stream point i, leads to

$$D_i = \tfrac{1}{8}\{3(\zeta_{i+1} - \zeta_{i+n+1}) + 6(\zeta_i - \zeta_{i+n}) - (\zeta_{i-1} - \zeta_{i+n-1})\}. \tag{24}$$

Here, ζ_{i+1} and ζ_{i+n+1} are fictitious elevations exterior to the sea area; eliminating $\zeta_{i+1} - \zeta_{i+n+1}$ by use of (23), yields (22.4). The expression for D_i given by (22.5) is obtained similarly.

To derive the D_i of (22.6), referring to figure 5 b, we write

$$\zeta_{i+n+1} - \zeta_{i+n} = \tfrac{1}{2}(E_i + E_{i+n}), \quad E_{i-n} = 2E_i - E_{i+n}, \quad \zeta_{i+1} - \zeta_i = \tfrac{1}{2}(E_i + E_{i-n})$$

and therefore

$$\zeta_{i+1} - \zeta_{i+n+1} = \zeta_i - \zeta_{i+n} + E_i - E_{i+n}. \tag{25}$$

A three-point interpolation as before, combined with (25), yields (22.6). The expressions given by (22.7), (22.8) and (22.9) are obtained in the same way.

The above use of a three-point Lagrange formula ensures, for the interpolated D_i, continuity with corresponding elevation-differences in the interior of the sea and a degree of consistency with the E_i given by (22.3).

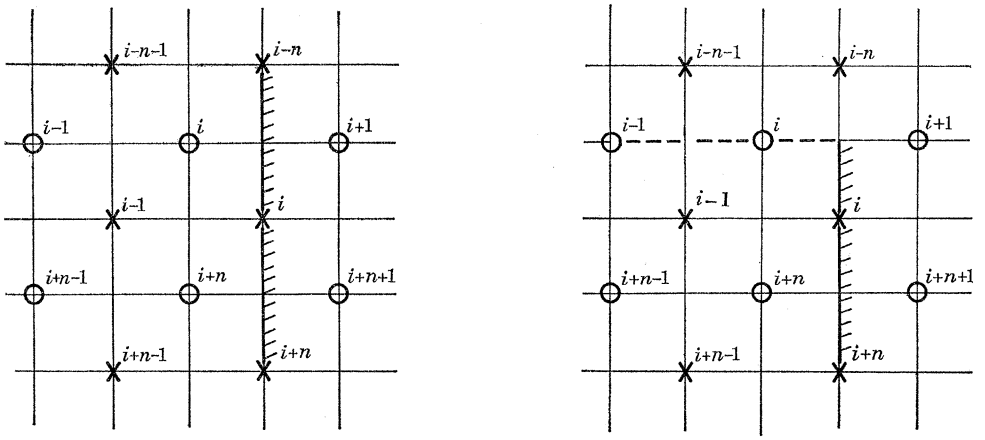

FIGURE 5. Stream point i on a longitudinal coastal boundary with (a) land to the east, and (b) land to the east and an open boundary to the north; sea / land, coastal boundary; ----○--, open-sea boundary.

Next we consider a stream point i on a latitudinal section of boundary (figures 3h to m). The coastal condition is now

$$U_i = 0 \tag{26.1}$$

and hence, from (20.1) and (20.2),

$$V_i(t+\tau) = (1-\tau\lambda_i)V_i(t) - \frac{\tau\beta h_i E_i(t)}{2\cos\phi_{2k}\Delta\chi} + \tau\gamma Q_i(t), \tag{26.2}$$

$$D_i = \frac{-2\omega\sin\phi_{2k}V_i + \gamma P_i}{\beta h_i/2\Delta\phi}. \tag{26.3}$$

Forms for E_i in (26.2) are determined by the same methods as those employed in the derivations of (22.4) to (22.9). The results may be set out as follows:

Stream point i on a latitudinal boundary,

with land to the south (figure 3h):

$$E_i = \tfrac{1}{16}\{18(\zeta_{i+1}-\zeta_i) - 2(\zeta_{i-n+1}-\zeta_{i-n}) - 3(D_{i+1}-D_{i-1})\}, \tag{26.4}$$

with land to the north (figure 3i):

$$E_i = \tfrac{1}{16}\{18(\zeta_{i+n+1}-\zeta_{i+n}) - 2(\zeta_{i+2n+1}-\zeta_{i+2n}) + 3(D_{i+1}-D_{i-1})\}, \tag{26.5}$$

with land to the south and an open boundary to the west (figure 3j):

$$E_i = \tfrac{1}{8}\{9(\zeta_{i+1}-\zeta_i) - (\zeta_{i-n+1}-\zeta_{i-n}) + 3(D_i-D_{i+1})\}, \tag{26.6}$$

with land to the north and an open boundary to the west (figure 3k):

$$E_i = \tfrac{1}{8}\{9(\zeta_{i+n+1}-\zeta_{i+n}) - (\zeta_{i+2n+1}-\zeta_{i+2n}) - 3(D_i-D_{i+1})\}, \tag{26.7}$$

with land to the south and an open boundary to the east (figure 3*l*):

$$E_i = \tfrac{1}{8}\{9(\zeta_{i+1}-\zeta_i)-(\zeta_{i-n+1}-\zeta_{i-n})-3(D_i-D_{i-1})\}, \tag{26.8}$$

with land to the north and an open boundary to the east (figure 3*m*):

$$E_i = \tfrac{1}{8}\{9(\zeta_{i+n+1}-\zeta_{i+n})-(\zeta_{i+2n+1}-\zeta_{i+2n})+3(D_i-D_{i-1})\}. \tag{26.9}$$

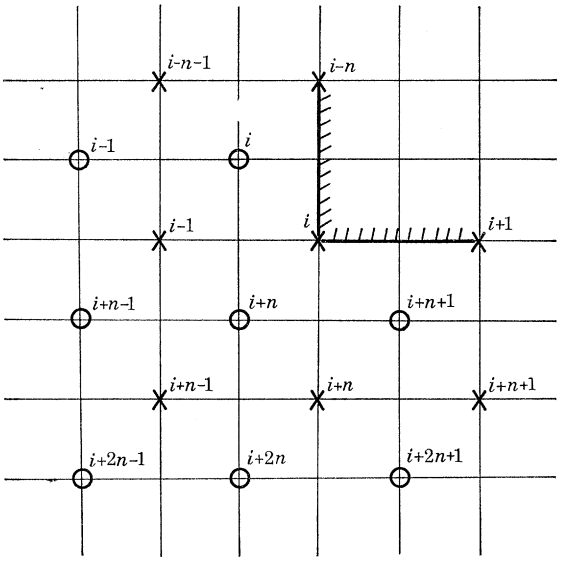

FIGURE 6. Stream point i at the apex of a 270° sector of sea with land in the northeast quadrant.

Finally, when the stream point i is a corner point at the apex of a 270° sector of sea (figures 3*n* to *q*) it is assumed that U_i, V_i are not generally zero and satisfy (20.1), (20.2). In such cases, the D_i and E_i for use in the latter equations are taken thus:

Stream point i at a 270° corner of the boundary

with land in the northeast quadrant (figure 3*n*):

$$D_i = \tfrac{1}{5}\{D_{i+1}+5(\zeta_i-\zeta_{i+n})-(\zeta_{i-1}-\zeta_{i+n-1})\}, \tag{27.1}$$

$$E_i = \tfrac{1}{5}\{E_{i-n}+5(\zeta_{i+n+1}-\zeta_{i+n})-(\zeta_{i+2n+1}-\zeta_{i+2n})\}, \tag{27.2}$$

with land in the southeast quadrant (figure 3*o*):

$$D_i = \tfrac{1}{5}\{D_{i+1}+5(\zeta_i-\zeta_{i+n})-(\zeta_{i-1}-\zeta_{i+n-1})\}, \tag{27.3}$$

$$E_i = \tfrac{1}{5}\{E_{i+n}+5(\zeta_{i+1}-\zeta_i)-(\zeta_{i-n+1}-\zeta_{i-n})\}, \tag{27.4}$$

with land in the southwest quadrant (figure 3*p*):

$$D_i = \tfrac{1}{5}\{D_{i-1}+5(\zeta_{i+1}-\zeta_{i+n+1})-(\zeta_{i+2}-\zeta_{i+n+2})\}, \tag{27.5}$$

$$E_i = \tfrac{1}{5}\{E_{i+n}+5(\zeta_{i+1}-\zeta_i)-(\zeta_{i-n+1}-\zeta_{i-n})\}, \tag{27.6}$$

with land in the northwest quadrant (figure 3*q*):

$$D_i = \tfrac{1}{5}\{D_{i-1}+5(\zeta_{i+1}-\zeta_{i+n+1})-(\zeta_{i+2}-\zeta_{i+n+2})\}, \tag{27.7}$$

$$E_i = \tfrac{1}{5}\{E_{i-n}+5(\zeta_{i+n+1}-\zeta_{i+n})-(\zeta_{i+2n+1}-\zeta_{i+2n})\}. \tag{27.8}$$

As an example of the derivation of these formulae, consider the case when there is land in the northeast quadrant. With reference to figure 6, which shows the stream point i and neighbouring

grid points of the sea, a three-point Lagrange interpolation between $\zeta_{i-1}-\zeta_{i+n-1}$, $\zeta_i-\zeta_{i+n}$ and D_{i+1}, evaluation being made on the line of longitude through the point i, yields (27.1). A similar interpolation between $\zeta_{i+2n+1}-\zeta_{i+2n}$, $\zeta_{i+n+1}-\zeta_{i+n}$ and E_{i-n}, making evaluation on the parallel of latitude through the point i, yields (27.2).

The difference equations (20), (21), (22), (26), (27) form the basis of an iterative procedure for the development of numerical solutions of the dynamical equations (6), (7), (8). The procedure is described in § 5 which follows. Solutions thus obtained represent surge motion in the model sea.

5. The iterative procedure

The flow diagram of figure 7 illustrates the computational method of the present work. The operation represented by the loop in the figure is applied successively for $t = 0, \tau, 2\tau, 3\tau$, etc., up to, say, $(m-1)\tau$ and, as a result, the ζ_i, U_i, V_i are determined at times $\tau, 2\tau, 3\tau, \ldots, m\tau$, starting from a knowledge of their values at time zero. Thus, by carrying out m iterations, the changing distribution of ζ_i, U_i, V_i over the sea is found numerically for the period $0 \leqslant t \leqslant m\tau$. Storm surge heights are given by ζ_i.

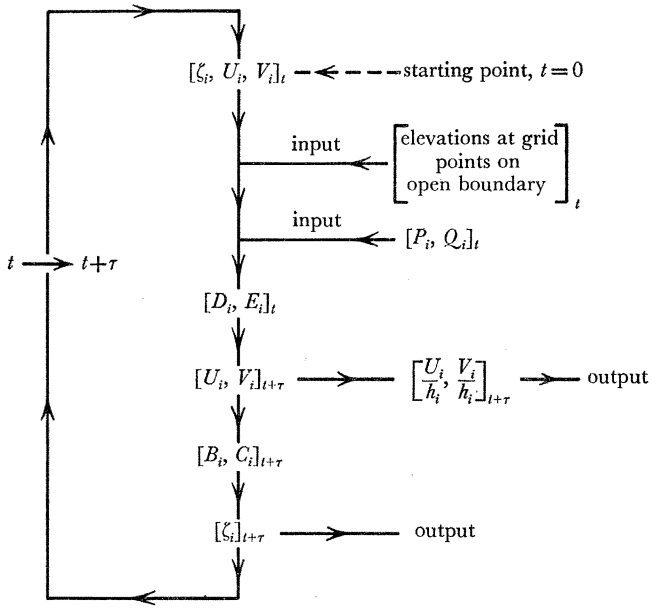

Figure 7. Flow diagram showing the computational method; D_i, E_i, U_i, V_i are evaluated at each stream point i within or on the boundary of the model sea and B_i, C_i, ζ_i at each elevation point i within the sea.

Since it is assumed, for convenience, that surges are generated from an initial state of rest, the iterative procedure described above is started by taking $\zeta_i = U_i = V_i = 0$ everywhere at $t = 0$. At the commencement of each time-step $(t, t+\tau)$, elevations ζ_i are prescribed at every elevation point i on the open boundary of the model sea and wind stress components P_i, Q_i at every stream point i within the sea or on its coastal boundary. The variations of elevation and wind stress thus specified define the surge-generating forces applied to the sea. With condition (12) in the North Sea investigations discussed later, $\zeta_i = 0$ at points i on the open boundary for all time.

For the purposes of the computations, the grid points are considered in 22 groups—corresponding respectively to the integer labels 1 to 22 defined in § 3. The points in any one group bear the same label, r say, and are numbered $s = 1, 2, 3, \ldots, N_r$, where N_r denotes the total number of points in the group. Thus, each grid point may be specified by the label r of the group to which it belongs and by an integer s giving its position within that group. The i, k associated with each point are related to the r, s of the point through suffixed variables:

$$i = c^{(i)}_{b+s}, \quad k = c^{(k)}_{b+s}, \tag{28.1}$$

where

$$b = A_r, \tag{28.2}$$

the A_r being defined by

$$A_1 = 0, \quad A_{q+1} = A_q + N_q \quad (q = 1, 2, 3, \ldots, 21). \tag{28.3}$$

The sequence of calculations indicated in figure 7, represented by

$$[\zeta_i, U_i, V_i]_t \rightarrow [D_i, E_i]_t \rightarrow [U_i, V_i]_{t+\tau} \rightarrow [B_i, C_i]_{t+\tau} \rightarrow [\zeta_i]_{t+\tau} \tag{29}$$

is carried out for the various grid points i of the model sea taken group-by-group in the order given by

$$r = 5\,(1)\,22,\ 6\,(1)\,17,\ 3: \quad s = 1\,(1)\,N_r \quad \text{for each} \quad r. \tag{30}$$

The calculations, involving a distinctive operation for each succeeding group of points, may be listed, in order of execution, as follows:

$r = 5$: D_i, E_i from (21.2)
6 (1) 11: E_i from (22.3)
12 (1) 17: D_i from (26.3)
18 (1) 21: D_i, E_i from (27.1) to (27.8); $[U_i, V_i]_{t+\tau}$ from (20.1), (20.2)
22 : D_i, E_i from (19); $[U_i, V_i]_{t+\tau}$ from (20.1), (20.2)
6 (1) 11: D_i from (22.4) to (22.9), $[U_i]_{t+\tau}$ from (22.2)
12 (1) 17: E_i from (26.4) to (26.9), $[V_i]_{t+\tau}$ from (26.2)
3 : $[B_i, C_i]_{t+\tau}$ from (16), $[\zeta_i]_{t+\tau}$ from (20.3)

Quantities are evaluated at time t apart from those with suffix $t+\tau$ which are evaluated at time $t+\tau$. Since the entire set of operations is ordered by varying r and s, the i, k values required in the difference equations are obtained from (28.1). In accordance with (21.1), (22.1) and (26.1), the following values are set permanently to zero: U_i and V_i for each point i in group 5, V_i for each point i in groups 6 to 11, and U_i for each point i in groups 12 to 17.

It should be noted that D_i, E_i are first determined from equations (21.2), (22.3), (26.3), which values are then used in the evaluation of the D_i, E_i given by equations (27.1) to (27.8), (22.4) to (22.9), (26.4) to (26.9).

6. The algol program

A computer program, written in ALGOL for an English Electric KDF 9 installation of 32 K core storage capacity, has been designed to carry out the sea-model calculations described in § 5.

The geometrical characteristics of the model sea are defined in the program data. This allows surge investigations to be carried out for sea basins of different shapes and sizes by merely altering the values of certain input parameters. Given the basic rectangular grid, these parameters consist

of the depths h_i and, specifying the boundary configuration of the model, the array of integer labels defined in § 3 (e.g. see table 1).

Each run of the program calculates elevations ζ_i and depth-mean currents U_i/h_i, V_i/h_i induced by wind acting over the model sea during a period $0 \leqslant t \leqslant m\tau$ corresponding to m time-steps. Input data specifies wind velocities over the sea surface throughout the period. The form of this data is now described.

The area of the model sea is divided up into subareas numbered $s' = 1, 2, 3, \ldots, S'$. A sequence of integers denoted by w_i $(i = 1, 2, 3, \ldots, np)$ identifies the subarea in which any particular stream point is located. Thus, $w_i = s'$ if stream point i lies within area s'. To complete the sequence we take $w_i = 0$ if stream point i lies outside the boundary of the sea.

Further, the period $m\tau$ covered by the computer run is divided up into consecutive intervals numbered $r' = 1, 2, 3, \ldots, R'$. Each interval is of duration τ_0 $(= m_0\tau)$ corresponding to m_0 time-steps, so that $m_0 R' = m$. Thus, for the interval r', we have $(r'-1)\tau_0 \leqslant t < r'\tau_0$.

During each interval it is supposed that both wind speed and wind direction are constant and uniformly distributed over each constituent area. Wind conditions over the surface of the model sea are then defined by

$$v_{r',s'}, \quad a_{r',s'} \quad (s = 1, 2, 3, \ldots, S';\ r' = 1, 2, 3, \ldots, R'),$$

where $v_{r',s'}$ denotes the wind speed and $a_{r',s'}$ the wind veer from the south, over the area s' during the interval r'. The $v_{r',s'}$ and $a_{r',s'}$, constant values, are obtained by averaging the natural variations of wind speed and wind veer over area s' during interval r'. The natural variations are derived on the basis of geostrophic winds extracted from meteorological charts.

The meteorological input data consists of matrices $[v_{r',s'}]$, $[a_{r',s'}]$. In the step $(t, t+\tau)$ of the iterative procedure, where $(r'-1)\tau_0 \leqslant t < r'\tau_0$, the program determines the wind-stress components P_i, Q_i from the relations

$$P_i = T_{r',s'} \cos a_{r',s'}, \quad Q_i = T_{r',s'} \sin a_{r',s'} \quad (s' = w_i). \tag{31}$$

Here, $T_{r',s'}$ denotes the resultant wind stress over area s' during interval r' calculated, in dynes/square centimetre, from the formula

$$T_{r',s'} = 2.4976 c v_{r',s'}^2, \tag{32.1}$$

where $v_{r',s'}$ is in miles/hour and the drag-coefficient c is given by

$$10^3 c = \left\{ \begin{array}{ll} 0.554 & \text{for} \quad v_{r',s'} \leqslant 11 \\ -0.12 + 0.06124 v_{r',s'} & \text{for} \quad 11 < v_{r',s'} < 43 \\ 2.513 & \text{for} \quad v_{r',s'} \geqslant 43 \end{array} \right\}. \tag{32.2}$$

The relations (32.1) and (32.2), expressing wind stress in terms of surface wind speed, are essentially those used by the author in previous investigations (Heaps 1965; Heaps & Ramsbottom 1966).

7. Stability

The stability of the finite-difference scheme is examined following the procedure employed by Fischer (1959). Assessment is thereby made of 'stability in the large', disregarding boundary conditions.

For simplicity, the dynamical equations are expressed in terms of rectangular Cartesian coordinates x, y, and are considered with constant coefficients and vanishing external forces. Thus,

$$\left.\begin{aligned}\frac{\partial U}{\partial t} &= -\lambda U + fV - gh\frac{\partial \zeta}{\partial x},\\ \frac{\partial V}{\partial t} &= -\lambda V - fU - gh\frac{\partial \zeta}{\partial y},\\ \frac{\partial \zeta}{\partial t} &= -\left(\frac{\partial U}{\partial x}+\frac{\partial V}{\partial y}\right),\end{aligned}\right\} \tag{33}$$

where $\lambda\ (=\kappa/h)$, $f\ (=2\omega\sin\phi)$ and h are regarded as constants. The direction of x increasing corresponds to that of ϕ increasing, and the direction of y increasing to that of χ decreasing; U, V are the x, y components, respectively, of the total stream.

The difference equations, approximating to (33), may be written

$$\begin{aligned}U^{t+\Delta t}_{x,y} &= (1-\lambda\Delta t)\,U^{t}_{x,y} + f\Delta t V^{t}_{x,y}\\ &\quad - gh(\Delta t/4\Delta x)\{\zeta^{t}_{x+\Delta x,y+\Delta y} - \zeta^{t}_{x-\Delta x,y+\Delta y} + \zeta^{t}_{x+\Delta x,y-\Delta y} - \zeta^{t}_{x-\Delta x,y-\Delta y}\}, \qquad (34)\\ V^{t+\Delta t}_{x,y} &= (1-\lambda\Delta t)\,V^{t}_{x,y} - f\Delta t U^{t}_{x,y}\\ &\quad - gh(\Delta t/4\Delta y)\{\zeta^{t}_{x+\Delta x,y+\Delta y} - \zeta^{t}_{x+\Delta x,y-\Delta y} + \zeta^{t}_{x-\Delta x,y+\Delta y} - \zeta^{t}_{x-\Delta x,y-\Delta y}\}, \qquad (35)\\ \zeta^{t+\Delta t}_{x,y} &= \zeta^{t}_{x,y}\\ &\quad - (\Delta t/4\Delta x)\{U^{t+\Delta t}_{x+\Delta x,y+\Delta y} - U^{t+\Delta t}_{x-\Delta x,y+\Delta y} + U^{t+\Delta t}_{x+\Delta x,y-\Delta y} - U^{t+\Delta t}_{x-\Delta x,y-\Delta y}\}\\ &\quad - (\Delta t/4\Delta y)\{V^{t+\Delta t}_{x+\Delta x,y+\Delta y} - V^{t+\Delta t}_{x+\Delta x,y-\Delta y} + V^{t+\Delta t}_{x-\Delta x,y+\Delta y} - V^{t+\Delta t}_{x-\Delta x,y-\Delta y}\}, \qquad (36)\end{aligned}$$

where elevations and streams are evaluated at the intersection points of a uniform rectangular (x,y)-grid with mesh dimensions Δx, Δy; Δt is an elementary time increment. Subscripts and superscripts denote, respectively, position and time of evaluation on the grid.

For the purposes of a stability analysis, the variables U, V, ζ are assumed to be periodic in space, proportional to $\exp\{\mathrm{i}(k_1x+k_2y)\}$ where k_1 and k_2 are real. An amplification matrix, relating U, V, ζ at $t+\Delta t$ to U, V, ζ at t, is subsequently derived from equations (34) to (36). The roots of the characteristic equation associated with this matrix lie within unit circle of the complex plane, centre at the origin, if

$$a^2+b^2 < 2-\lambda\Delta t+2(1-\lambda\Delta t+f^2\Delta t^2)^{\frac{1}{2}} \tag{37}$$

and

$$\Delta t < \lambda/f^2, \tag{38}$$

where

$$a=\sqrt{(gh)}\,\frac{\Delta t}{\Delta x}\sin k_1\Delta x\cos k_2\Delta y, \quad b=\sqrt{(gh)}\,\frac{\Delta t}{\Delta y}\sin k_2\Delta y\cos k_1\Delta x. \tag{39}$$

Apart from the presence of the factors $\cos k_2\Delta y$, $\cos k_1\Delta x$ in (39), the above results correspond closely to those derived by Fischer. The factors arise because of the use of *averaged* space differences in the difference equations.

Approximately, (37) gives $a^2+b^2<4$, which, on using (39), may be written

$$gh\Delta t^2\left(\frac{\sin^2 k_1\Delta x\cos^2 k_2\Delta y}{\Delta x^2}+\frac{\sin^2 k_2\Delta y\cos^2 k_1\Delta x}{\Delta y^2}\right)<4.$$

This is satisfied for all k_1, k_2 provided that

$$\Delta t < 2(gh)^{-\frac{1}{2}}\min(\Delta x,\Delta y), \tag{40}$$

where min indicates that the minimum of Δx and Δy is taken.

Hence, according to basic theory discussed by Fischer, (38) and (40) are conditions for stability in the Cartesian plane. Applying them to the actual difference scheme on the spherical Earth, reverting to the notation of preceding sections, we can formulate stability criteria as follows:

$$\tau < L\left\{\frac{\kappa}{h4\omega^2\sin^2\phi}\right\}, \tag{41}$$

$$\tau < L\{2(gh)^{-\frac{1}{2}}\min(a\Delta\phi, a\cos\phi\Delta\chi)\}, \tag{42}$$

where L denotes that a lower bound is taken—considering the variations of h and ϕ over the entire area of the model sea. As stated by Harris & Jelesnianski (1965), conditions such as (41) and (42) provide only a *guide* to stability in practice, because of the simplifying assumptions made in their derivation.

It seems appropriate at this point to make some general comments on our scheme of differences. An important feature is the use of forward and backward differences in time, enabling field values at time $t+\tau$ to be deduced directly from those at time t. This is in contrast to the commonly used schemes involving central time differences, where field values at *two* earlier time levels $t-\tau$, t are normally required to determine further values at $t+\tau$—as described, for example, by Harris & Jelesnianski (1964). The present scheme does not suffer from the disadvantage of an implicit scheme (such as that used by Uusitalo 1960) in having to solve algebraic equations, or carry out an iterative process, in the performance of each cycle of the time-stepping sequence.

However, condition (41) indicates that a certain level of friction, at least, is required for stability. Generally, this is an undesirable limitation, although for relatively shallow sea areas, such as those considered in this paper, experience so far has shown it to be acceptable. Fairly recent developments (Fischer 1965; Sielecki 1968) suggest that, by slightly modifying the difference equations, the restriction represented by (41) may be removed. For the purposes of illustration we consider these modifications as applied to equations (34) to (36). On the one hand, adopting proposals put forward by Fischer (1965), the geostrophic terms are centred in time so that $f\Delta tV^t_{x,y}$ and $-f\Delta tU^t_{x,y}$ are replaced by

$$\tfrac{1}{2}f\Delta t(V^t_{x,y}+V^{t+\Delta t}_{x,y}) \quad \text{and} \quad -\tfrac{1}{2}f\Delta t(U^t_{x,y}+U^{t+\Delta t}_{x,y})$$

respectively. The difference scheme then becomes implicit but only a system of two algebraic equations has to be solved for the unknowns $U^{t+\Delta t}_{x,y}$, $V^{t+\Delta t}_{x,y}$: in fact, the solutions may be expressed analytically, whence the system effectively returns to explicit form. On the other hand, incorporating the essentials of a scheme due to Sielecki (1968), the difference equations are set up as follows:

$$\begin{aligned}
\zeta^{t+\Delta t}_{x,y} &= \zeta^t_{x,y} \\
&\quad -(\Delta t/4\Delta x)\{U^t_{x+\Delta x,y+\Delta y}-U^t_{x-\Delta x,y+\Delta y}+U^t_{x+\Delta x,y-\Delta y}-U^t_{x-\Delta x,y-\Delta y}\} \\
&\quad -(\Delta t/4\Delta y)\{V^t_{x+\Delta x,y+\Delta y}-V^t_{x+\Delta x,y-\Delta y}+V^t_{x-\Delta x,y+\Delta y}-V^t_{x-\Delta x,y-\Delta y}\}, \\
U^{t+\Delta t}_{x,y} &= (1-\lambda\Delta t)\,U^t_{x,y}+f\Delta tV^t_{x,y} \\
&\quad -gh(\Delta t/4\Delta x)\{\zeta^{t+\Delta t}_{x+\Delta x,y+\Delta y}-\zeta^{t+\Delta t}_{x-\Delta x,y+\Delta y}+\zeta^{t+\Delta t}_{x+\Delta x,y-\Delta y}-\zeta^{t+\Delta t}_{x-\Delta x,y-\Delta y}\}, \\
V^{t+\Delta t}_{x,y} &= (1-\lambda\Delta t)\,V^t_{x,y}-f\Delta tU^{t+\Delta t}_{x,y} \\
&\quad -gh(\Delta t/4\Delta y)\{\zeta^{t+\Delta t}_{x+\Delta x,y+\Delta y}-\zeta^{t+\Delta t}_{x+\Delta x,y-\Delta y}+\zeta^{t+\Delta t}_{x-\Delta x,y+\Delta y}-\zeta^{t+\Delta t}_{x-\Delta x,y-\Delta y}\}.
\end{aligned}$$

Here, evaluations are carried out in the order indicated and the system is therefore explicit. From the computational point of view economy is achieved by the fact that no storage of old

fields is necessary—since after each field has been evaluated its previous values are not used in the remaining equations. Preliminary analyses confirm that, for either of the modified schemes, the presence of friction is no longer a requirement for stability. It appears that the geostrophic terms are sources of instability and that this influence is overcome by writing the terms in some degree implicitly.

8. Computation of North Sea surges

An account is now given of the application of the system of computation described in the preceding sections to the problem of North Sea storm surges. The results obtained are discussed subsequently in § 9.

(*a*) *North Sea models*

Three models of successively increasing size and complexity have been used to compute storm surges in the North Sea (figures 8 to 10). For each model, the mesh size is such that $\Delta\phi = \frac{1}{6}°$, $\Delta\chi = \frac{1}{4}°$. The distance between consecutive elevation (or stream) points, measured along a line of longitude, is 23.0 miles; the distance between consecutive points measured along a parallel of latitude ranges from 16.1 miles along the extreme northern boundary of the models to 23.2 miles along the southernmost boundary of models 2 and 3.

Table 2 shows the depth distribution (h_i) taken for model 3. Apart from a few values associated with stream points lying along the northwestern edge of the continental shelf, the same set also gives (inclusively) the depths used in models 1 and 2. From soundings on navigational charts, h_i was determined as a mean depth for the neighbourhood surrounding the stream point i. The various h_i obtained in this way were then smoothed graphically after cross-plotting with reference to the lines of the finite-difference grid. Table 2 presents the smoothed values.

Subareas used in specifying wind conditions over the respective models are shown in figures 11 (*a* to *c*). The areas—which correspond to those employed by the Meteorological Office for weather forecasts—are numbered as indicated in the figures. As input data for surge calculations, surface winds over the different areas were determined for consecutive 2 h intervals, following the general pattern set out in § 6. The wind data were prepared by the Meteorological Office by extracting geostrophic winds from 1 : 3 000 000 hourly weather charts of the British Isles: the geostrophic winds were then adjusted to surface winds by using results obtained by Findlater *et al.* (1966). Final estimates of the surface values took into consideration ships' observations and a few land observations, particularly on occasions when the curvature of the isobars appeared to be significant.

In computations using models 1 and 2 the time-step τ in the iterative procedure was taken as 0.1 h. It was found that this choice ensured stable solutions and satisfactory convergence with respect to time-step length. The stability criteria (41) and (42) are satisfied, albeit (41) marginally so. Computations based on model 3 were carried out with $\tau = 0.05$ h, τ being necessarily smaller than before because of the greater maximum depth. In these circumstances, condition (42) is again satisfied but (41) is not, since τ now exceeds $\kappa/h4\omega^2\sin^2\phi$ at stream points where the depth is greater than 450 fathoms. Such points are few in number, covering a relatively small region of the model, and therefore it seems reasonable to conclude that any latent instability associated with them is effectively countered by the overall stability. Thus, while (41) may be a sufficient condition for stability, the indications are that it is certainly not a necessary one.

PHILOSOPHICAL TRANSACTIONS OF THE ROYAL SOCIETY A MATHEMATICAL, PHYSICAL & ENGINEERING SCIENCES

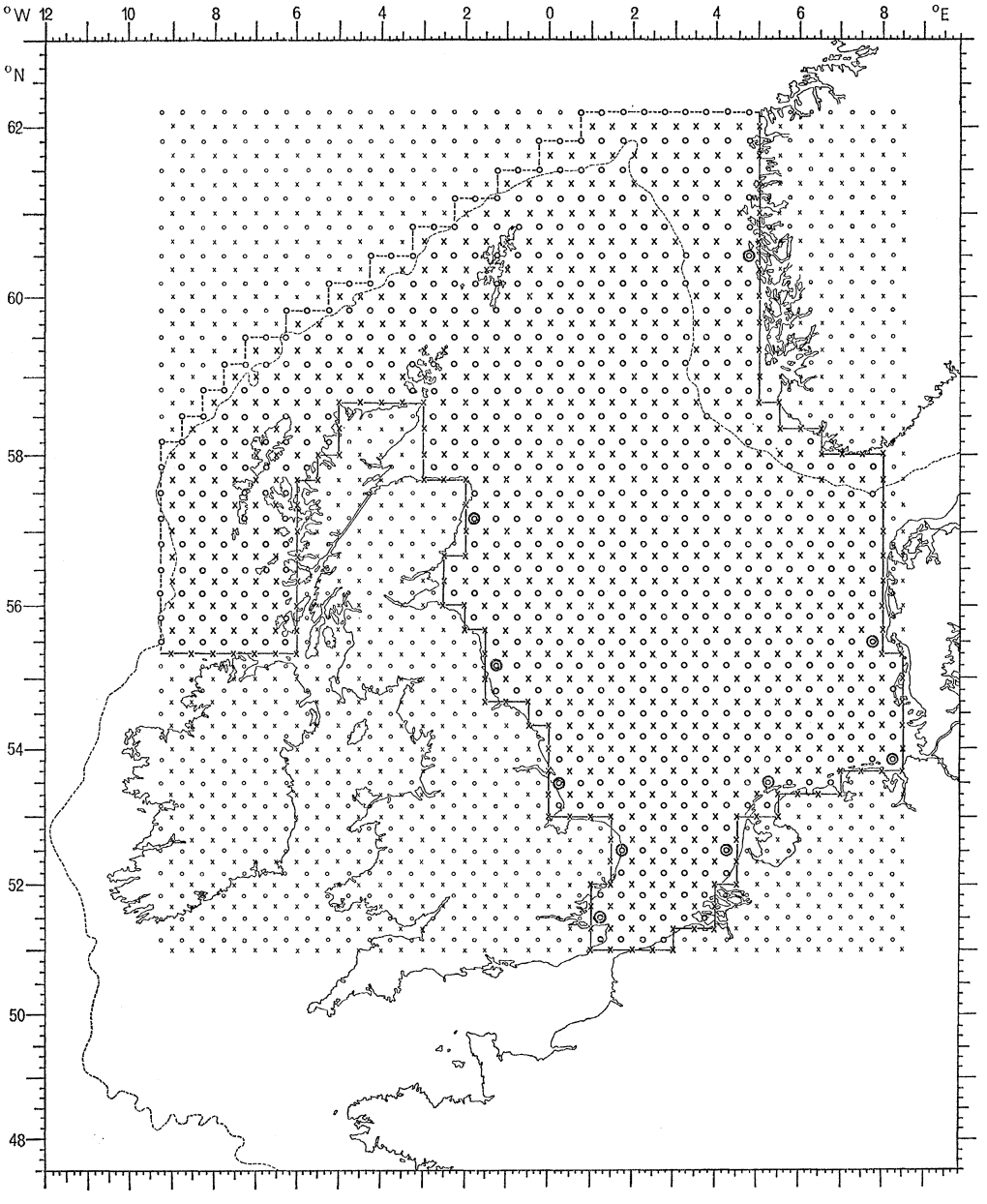

FIGURE 8. Model 1, covering the North Sea and northern shelf areas, the Strait of Dover closed; ––○––, open boundary; —×—, closed boundary; ------, 100 fathoms; ◎, point at which calculated elevations are compared with elevations derived from observations at a nearby port.

(*b*) *Surge cases*

The sea models described in § 8 (*a*) have been used to determine wind-induced elevations and currents for three different periods:

(i) 06.00 h 13 September to 12.00 h 15 September 1956

(ii) 12.00 h 24 February to 18.00 h 26 February 1958

(iii) 00.00 h 15 February to 00.00 h 18 February 1962

PHILOSOPHICAL TRANSACTIONS OF THE ROYAL SOCIETY A MATHEMATICAL, PHYSICAL & ENGINEERING SCIENCES

PHILOSOPHICAL TRANSACTIONS OF THE ROYAL SOCIETY A MATHEMATICAL, PHYSICAL & ENGINEERING SCIENCES

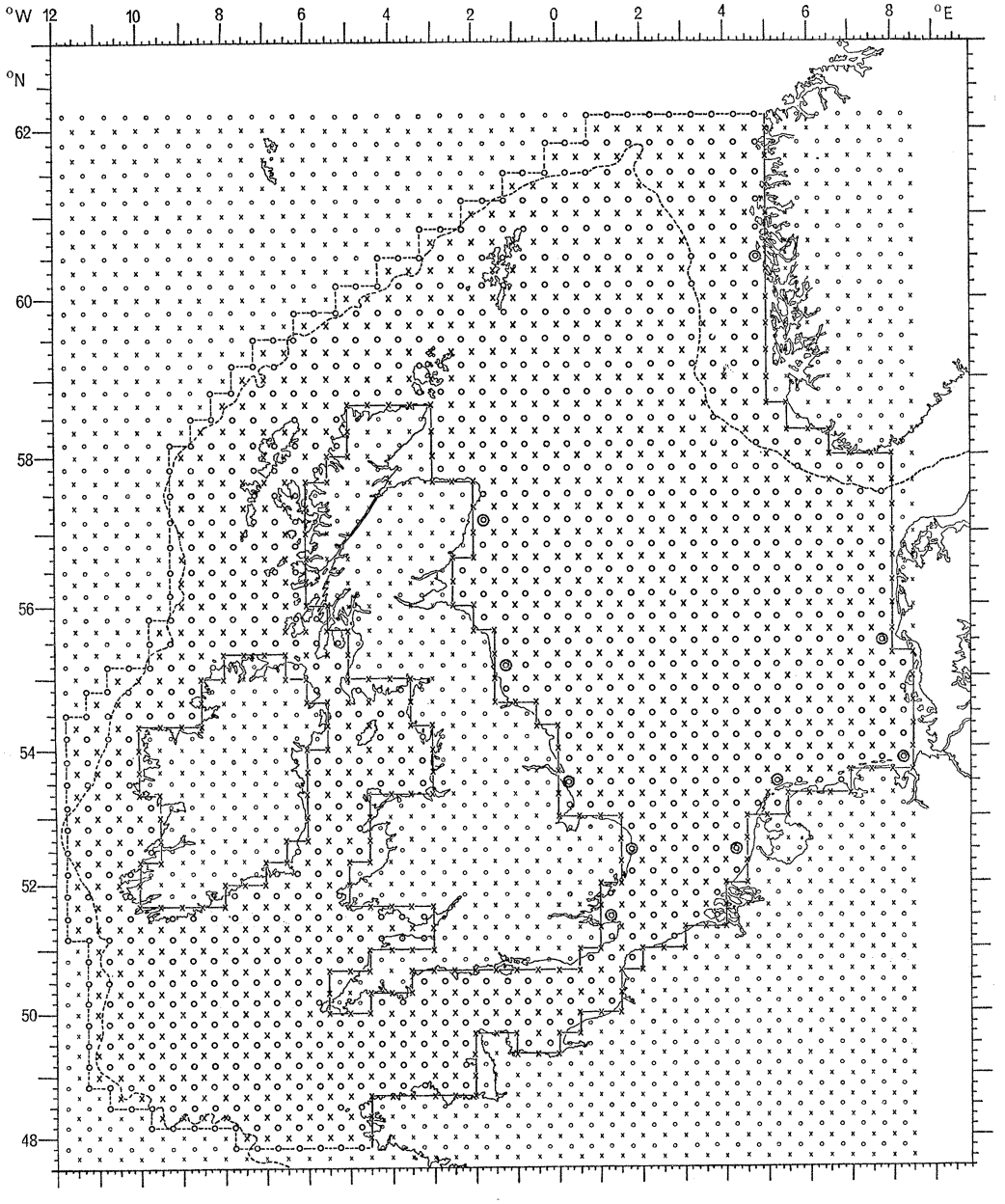

FIGURE 9. Model 2, covering the North Sea and shelf regions surrounding the British Isles; --○--, open boundary; —×—, closed boundary; ------, 100 fathoms; ◎, point at which calculated elevations are compared with elevations derived from observations at a nearby port.

covering, respectively, a typical external surge in the North Sea, a surge located in the southern North Sea, and a major North Sea surge (the so-called 'Hamburg' surge) in which levels in the German Bight were raised by over 11 ft. Time-stepping through each period, runs of the ALGOL program yielded an output of elevations and depth-mean currents every 2 h; concurrently, input of surface wind data occurred at 2 h intervals. A series of runs was carried out first with model 1, covering all three surge cases. Then followed a similar series with model 2. Finally, model 3 was used to make a further investigation of surge case (i). Results of the computations are presented in figures 14 to 17, 20, 21 and 24 to 26.

In figures 14, 20 and 24 comparisons are made between computed and observed wind surges for a number of places on the North Sea coast. Three variations are shown for each port—for each surge period. Considering any one of the ports, two of the variations shown represent the

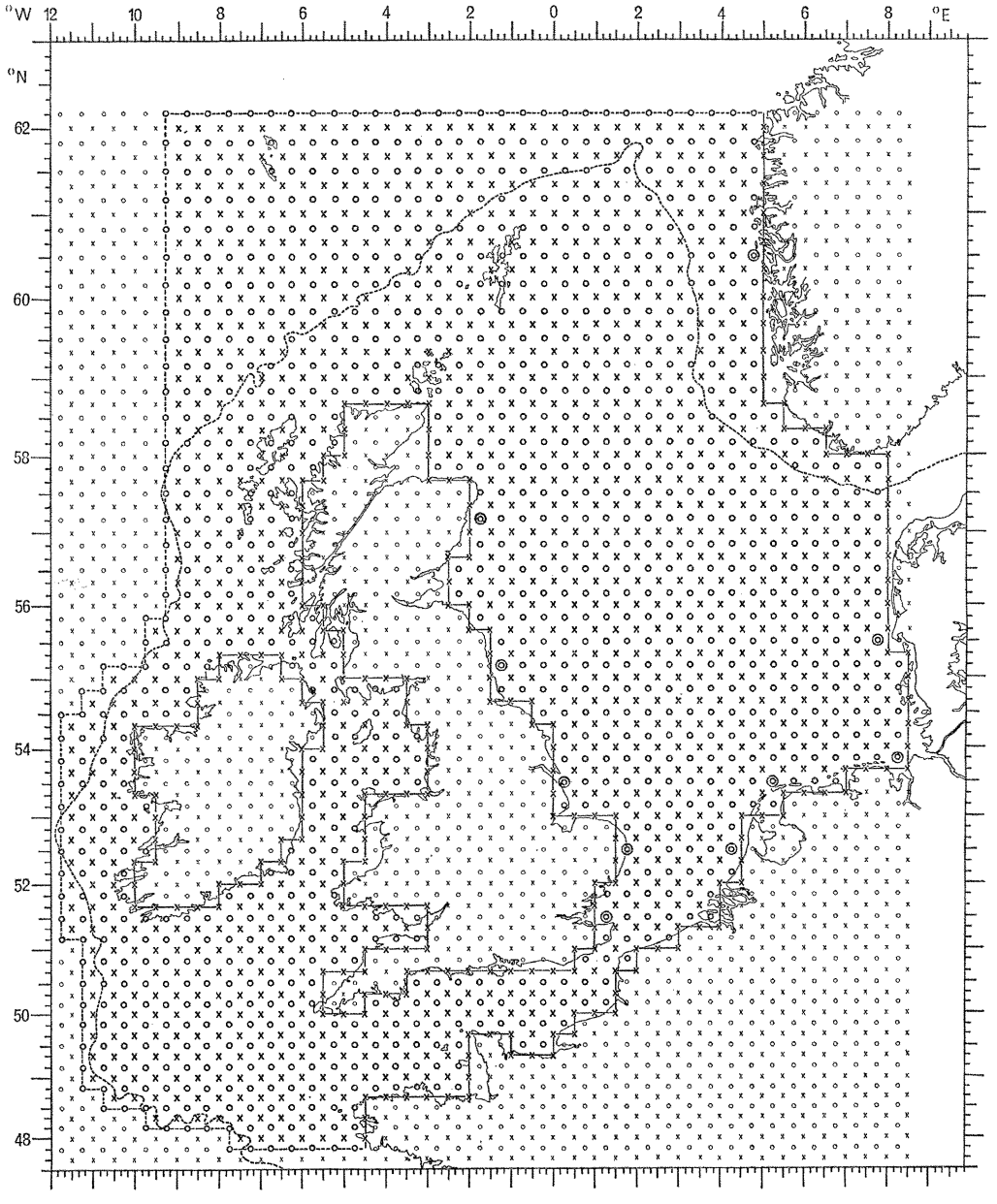

FIGURE 10. Model 3, covering the area of model 2 extended in the northwest to take in an area of oceanic water; –– ○ ––, open boundary; — × —, closed boundary; ------, 100 fathoms; ◎, point at which calculated elevations are compared with elevations derived from observations at a nearby port.

wind surges derived respectively from models 1 and 2 at a grid point in close proximity to that port. The third is obtained from sea-level observations at the port, being a plot of $\zeta_O - \zeta_T - \zeta_B$, where ζ_O is the observed elevation of the sea surface, ζ_T the astronomical tide obtained from orthodox methods of tidal prediction, and ζ_B the barometric surge estimated in terms of the

deviation of the local barometric pressure from its mean value using the well-known statical law—quoted, for example, by Charnock & Crease (1957) and Heaps (1967). In practice, starting with observed elevations, extraction of the tides yielded sea-level residuals, $\zeta_O - \zeta_T$, and removal of the barometric surge from these residuals then gave wind-surge estimates in the form of $\zeta_O - \zeta_T - \zeta_B$. Thus, for each port, the comparison presented by the figures is between, on the one hand, the two surge forms obtained from the sea-model calculations and, on the other hand, the surge estimated from observational data. The grid points, associated with the various ports, at which the computed surge forms were evaluated, are indicated by the double-circles in figures 8 to 10.

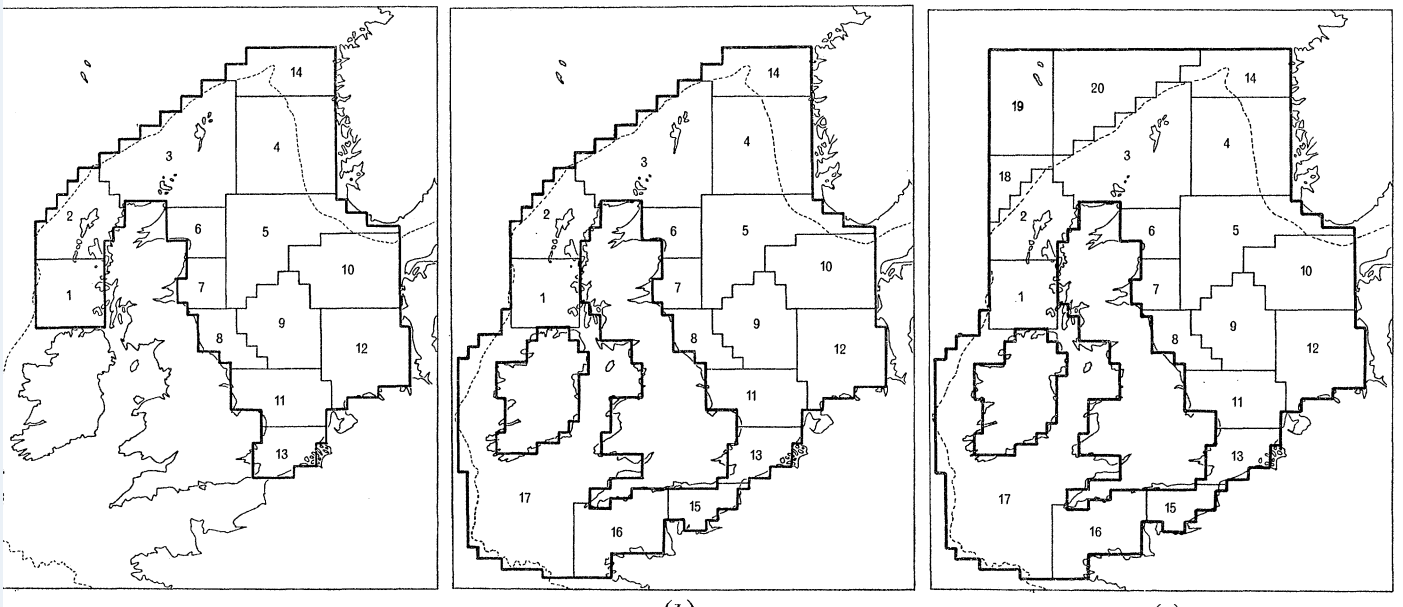

FIGURE 11. Subareas used in the specification of wind conditions over (*a*) model 1, (*b*) model 2, and (*c*) model 3.

From the outputs of elevation derived from the runs with model 1, co-disturbance lines have been drawn to show the changing spatial distribution of wind-induced surge level during the periods considered. The results appear in figures 16, 21, 25 and 26. Patterns of sea-level disturbance are given at 2 h intervals for the external surge (figure 16) and at 6 h intervals for the surge in the south of the North Sea (figure 21). Similar diagrams are given describing the first stages in the development of the major 'Hamburg' surge (figure 25) and the subsequent build-up and subsidence of this surge (figure 26). For the external surge, a further analysis of the computed elevations was carried out to determine (*a*) lines joining points at which maximum elevation occurred at the same time, and (*b*) contours of maximum elevation: counterparts, respectively, of co-tidal and co-range lines in tidal theory. Charts showing the distributions obtained are given in figure 17.

Although depth-mean components of current have been computed, these are regarded as being of subsidiary interest to the elevations. The emphasis is on the analysis of sea-level disturbances, this being the essence of the storm-surge problem. Detailed consideration of surge

currents is reserved for future investigations: it is hoped that such further work will include the dynamic effects of atmospheric pressure, as well as of wind, and determine the three-dimensional current structure.

(c) *Use of the 'influence method'*

On the basis of the 'influence method' described by Welander (1961), the system for calculating storm surges, operated by the ALGOL program, may be reformulated in general terms as follows.

Again consider surges generated in a period $0 \leqslant t \leqslant m\tau$, wind conditions over the model sea during this time being prescribed as in § 6. Let $\zeta_i(q, s', N)$ denote the elevation at the grid point i, at time $t = q\tau_0$, due to a uniform wind stress of 20 dyn/cm² directed to the *north* acting over the subarea s' during the interval $0 \leqslant t \leqslant \tau_0$. Similarly, let $\zeta_i(q, s', E)$ denote the elevation at the same point and time due to the same wind stress acting to the *east* over area s' during the interval $0 \leqslant t \leqslant \tau_0$. Consider $q = 1, 2, 3, \ldots, R'$ so that $0 < q\tau_0 \leqslant m\tau$. Then the sea-level response at point i and time $q\tau_0$, due to the prescribed sequence of wind fields acting over the model sea during the surge period, is given by

$$\zeta_i(t = q\tau_0) = \sum_{s'=1}^{S'} \sum_{r'=1}^{q} \tfrac{1}{20}[T_{r',s'} \cos a_{r',s'} \zeta_i(q - r' + 1, s', N) + T_{r',s'} \sin a_{r',s'} \zeta_i(q - r' + 1, s', E)], \tag{43}$$

where $T_{r',s'}$ is the resultant wind stress over area s' during interval r', determined in dynes/square centimetre from (32.1): $T_{r',s'} \cos a_{r',s'}$ and $T_{r',s'} \sin a_{r',s'}$ are its components directed to the north and to the east respectively.

In (43), the separate effects of the various wind fields have been superimposed to yield the total surge at a particular point and time. The sea-level responses $\zeta_i(q, s', N)$ and $\zeta_i(q, s', E)$ at each elevation point i of the model, at each time $q\tau_0$ ($q = 1, 2, 3, \ldots, R'$), associated with each area s' ($s' = 1, 2, 3, \ldots, S'$), may be regarded as basic data for storm-surge calculations. Taking an appropriate linear combination of these responses, as in (43), yields the surge, at regular intervals τ_0, corresponding to any particular set of meteorological conditions. The validity of such linear superposition rests on the linearity of the basic hydrodynamical equations since, effectively, the process is one of adding solutions.

Based on the above theory, a system for computing North Sea surges has been set up for model 1. Response functions $\zeta_i(q, s', N)$, $\zeta_i(q, s', E)$ have been determined from the basic ALGOL program to cover a surge period of 54 h, taking $\tau_0 = 2$ h and $R' = 27$. These determinations have been carried out for the different subareas of the model, for 62 different elevation points i distributed along the North Sea coast. Computations of the surge $\zeta_i(t = q\tau_0)$, given by (43), are performed by a separate ALGOL program which accepts the wind data (i.e. the $v_{r',s'}$ and $a_{r',s'}$ values) as input, reading the response functions from a permanent store in the form of magnetic tape. The system was applied first to surge case (i), then to surge case (ii), and it was verified that the surge values obtained at the selected coastal elevation points agreed with the corresponding values obtained from the sea-model calculations described in § 8 (*b*). Further to this, the surge contributions originating from the various subareas of the model sea were found. For case (i), the contributions to the total calculated wind surge off Aberdeen are plotted in figure 18 (*a*). For case (ii), the contributions to the total surge off Southend are plotted in figure 22 (*a*).

The use of response functions is an approach which lends itself to the routine operational prediction of storm surges, as shown by Jensen & Weywadt (1966) in their proposals for the forecasting of surge levels at ports along the Danish and German coasts. A point in favour of the

method is its ability to identify times and regions of surge generation by the determination of the surge components associated with different sea areas. However, from the experience gained in the present work, the approach was found to be largely unsuitable in carrying through a program of research and development. While economy was achieved in running-time on the computer, the preparation of the response functions and their installation on magnetic tape was found to be a major and onerous task. The end product was an inflexible system, since modifications to the sea model called for a new set of standard responses.

(*d*) *Scheme for calculating sea level*

The relevance of the sea-model computations, described in the preceding subsections, to the problem of calculating the variations in sea level at a coastal site, is shown in figure 12. The total elevation of the sea surface is assumed to consist of the predicted tide ζ_T, the wind surge ζ_W derived from computations, and the barometric surge ζ_B estimated from the statical law. Non-linear interactions of tide and surge, which may be significant in shallow coastal waters, are ignored. Also, no account is taken of possible dynamic effects produced by changes in barometric pressure over the sea surface.

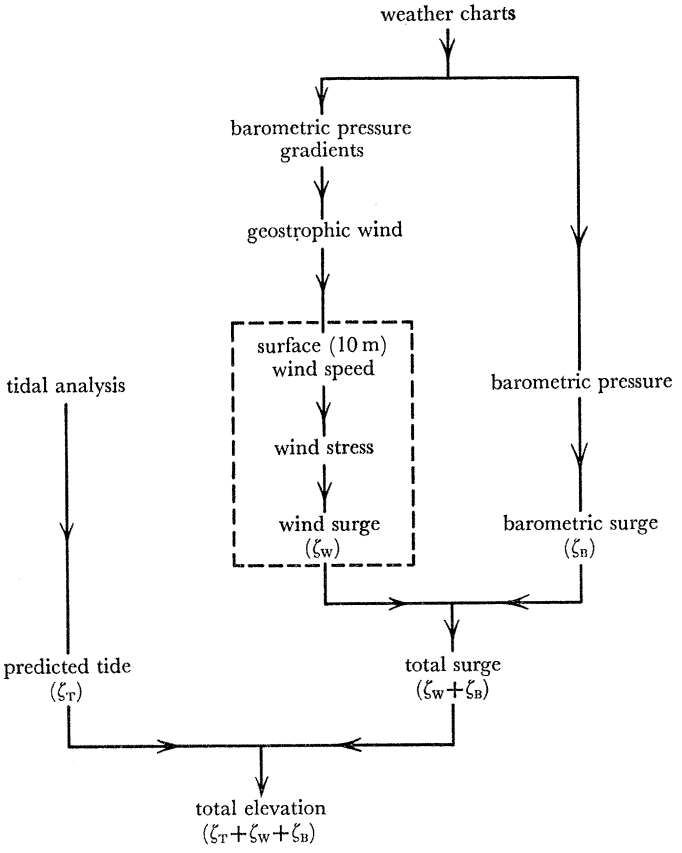

FIGURE 12. Scheme for calculating sea level; ⋯, sea-model computations.

Concerning the neglect of nonlinear effects, a further investigation is now in progress at the Tidal Institute in which these influences are specifically included in a numerical model of the southern North Sea. The hydrodynamical equations, in nonlinear form, are solved to determine

motion consisting of both tides and surges. The first stages of this project have already been completed (Banks 1967) and the final outcome will be reported in due course.

The credibility of the law of the static response of sea level to atmospheric pressure, for the North Sea, has been established mainly through the extensive use of the law in the derivation of empirical formulae for surge forecasting (Heaps 1967). However, Cartwright (1968) has produced evidence to show that, at Aberdeen, there is a departure from the static value of -1 cm/mb for disturbances with frequencies higher than 0.25 c/d. Clearly, there is scope for more research into this question and, to this end, it is intended that future work with the North Sea models will include consideration of the dynamic effects of pressure by retaining pressure gradients over the sea surface as forcing terms in the equations of motion. Such a step would, of course, increase even further the size and complexity of the numerical problem, and it was this additional burden which we sought to avoid—for the sake of simplicity—in the present work.

The extent of the agreement between the observed and calculated surge profiles shown in figures 14, 20 and 24 gives some indication of the efficacy of the scheme for sea-level calculation illustrated by figure 12.

9. Discussion of results

The results obtained from our sea-model computations are now examined in detail. For each of the three surge cases considered, the calculated surge values are discussed in relation to the appropriate meteorological conditions and surge heights deduced using sea-level observations. Figures 13 to 26 form the basis for the discussion.

(*a*) *External surge*, 13 *to* 15 *September* 1956

The meteorological conditions which produced this surge are shown by the weather charts of figure 13. During the period 06.00 h 13 September to 18.00 h 14 September, a depression passed from the Atlantic Ocean to the Norwegian Sea, its centre moving approximately northeastwards between Scotland and Iceland. Strong winds, associated with the depression, acted on the areas of shelf sea lying to the north and west of Scotland and to the north of the North Sea (areas 1, 2, 3, 4 in figure 11), but over most parts of the North Sea itself the weather situation was comparatively quiet. Accordingly, the resulting storm effects experienced in the North Sea must have been generated mainly outside its northern entrance.

The sea-level residuals, corrected for the effects of local barometric pressure and plotted in figure 14, show that a simple rise and fall in level travelled southwards down the east coast of the British Isles, exhibiting the characteristics of external-surge propagation established by Corkan (1948) and Rossiter (1959). An interesting feature of this and other external surges is that the rate of progression and variation in height of the surge maximum, from one east coast port to the next, are closely similar to the corresponding rates of progression and variations in amplitude of the major tidal constituents M_2, S_2, K_1, O_1; particularly is this true when considering the diurnal tides. The residuals at the continental ports indicate that a surge occurred there of quite different character to that recorded on the English coast. There is evidence of a surge progression from Ijmuiden to Cuxhaven taking the form of a rather weak indistinct reflexion of the incoming wave from the north. The levels at Cuxhaven were disturbed by the after-effects of a larger surge in the German Bight on 12 September.

Figure 14 shows that the computations were largely successful in reproducing the observed surges at Aberdeen, Tyne Entrance and Immingham. This suggests that the mechanism of surge

generation in the northern sea areas was satisfactorily represented in the numerical work. However, as is apparent from the figure, at Lowestoft and Southend the calculated surges turned out to be significantly smaller than those which were actually experienced. Tentative explanations for these underestimates may be put forward. Thus, it is conceivable that, in the model, too great a portion of the southwards-travelling surge was reflected at the northern coastline of East Anglia, as a result of which too small an amount of surge energy passed into the Southern Bight—producing smaller rises in level there than those which were observed. Another possible explanation is that the coarseness of the finite-difference grid prevented the computations from taking

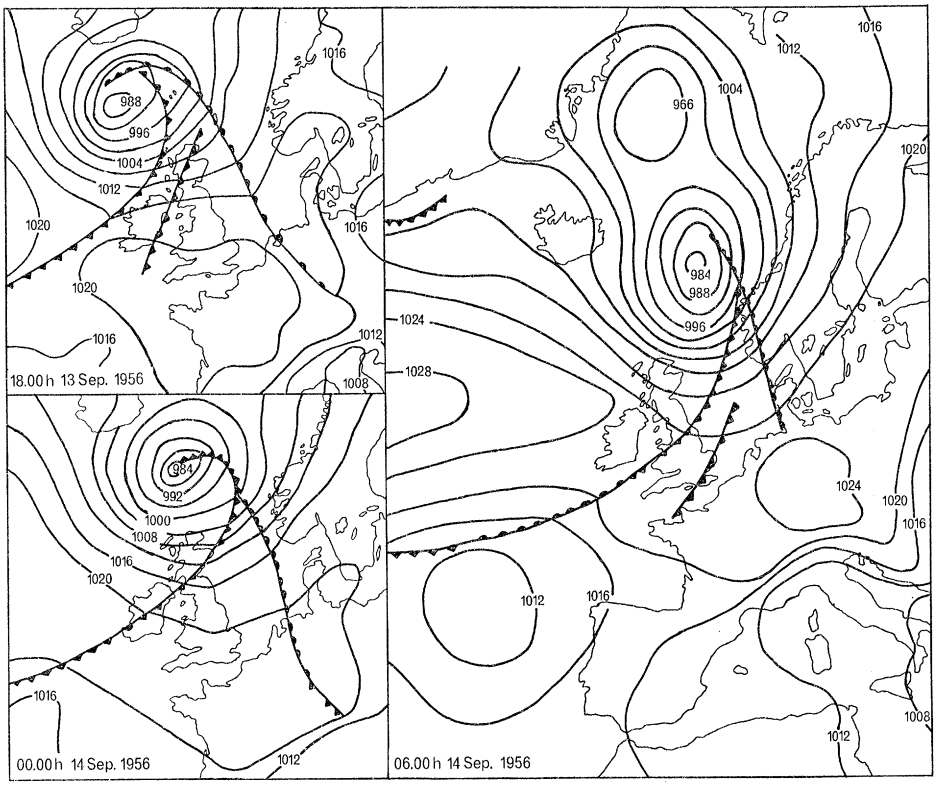

FIGURE 13. Weather charts for the storm surge of 13 to 15 September 1956.

full account of surge amplification in the shallow coastal waters off East Anglia: on this basis, future need is for a finer grid to define in greater detail the coastal depths and boundaries. Also, the neglect of nonlinear effects near the coast may have substantially affected the calculated results. Finally, in all these considerations, it has to be remembered that the computed surge values for a port refer to an elevation point lying some 10 miles off-shore and therefore, on this count alone, one must expect differences between observation and theory, particularly in rapidly shallowing areas. A further aspect of figure 14 shows the influence of the Strait of Dover on surge levels in the North Sea. The computed surge profiles (derived from model 1 with the Strait closed and from model 2 with the Strait open) indicate that flow through the Strait produced noticeable lowerings of level at Southend and Ijmuiden; farther north, the influence was unimportant.

PHILOSOPHICAL TRANSACTIONS OF THE ROYAL SOCIETY A MATHEMATICAL, PHYSICAL & ENGINEERING SCIENCES

A point of special interest in connexion with external surges in the North Sea is the extent to which their formation is determined by disturbances generated in the ocean and then propagated on to the continental shelf. To examine this question in relation to the present surge case, the variations in wind-induced elevation at the various North Sea ports during the period, as determined on the one hand from model 2 and on the other hand from model 3, have been compared. The results are shown in figure 15. It is apparent that the differences at each port

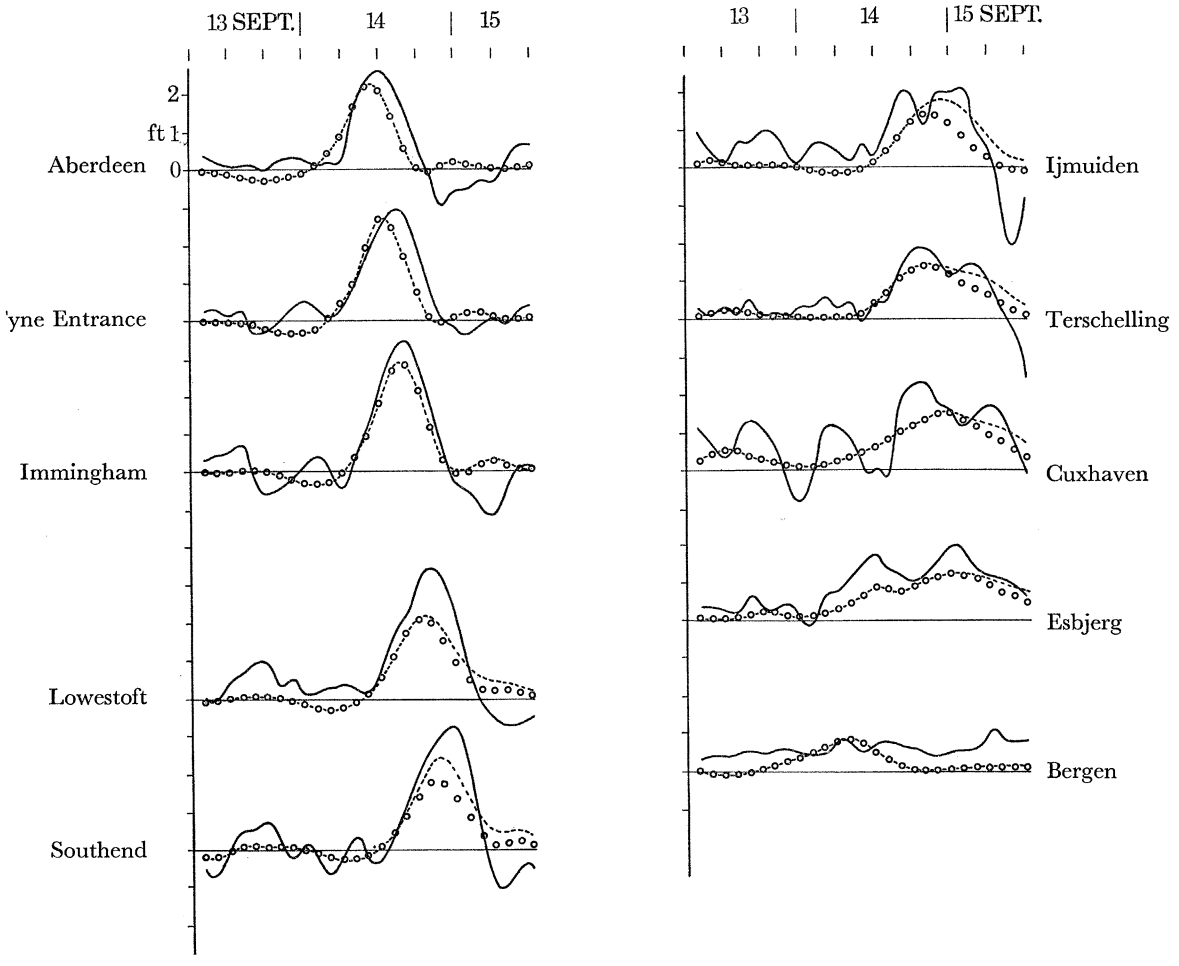

FIGURE 14. Storm surge of 13 to 15 September 1956; ——, residuals after removal of the barometric surge; ------, wind surge from model 1; ○, wind surge from model 2.

between the variations derived from the respective models are very small—indicating that the wind fields which acted over the oceanic areas 18, 19 and 20, lying off the northwestern edge of the shelf (figure 11*c*), had a negligible effect in the generation of the external surge. Hence, there are good grounds for believing that the surge was, for the most part, generated on the shelf, with little contribution from the ocean. This may well be true generally of external surges, for the present case is a fairly representative example. Further investigations are required using an extended 'oceanic' model, coupled with the marginal sea areas, in order to make a more complete study of meteorologically induced disturbances in the ocean and their effects on surface levels at coastal points.

The co-disturbance patterns of figure 16 describe the changing spatial distribution of wind-induced surge elevation between 20.00 h on 13 September and 12.00 h on 15 September. The variations shown may be summarized as follows. During 13 September there was a build-up of elevation centred on the northwest coast of Scotland due, fairly obviously, to south to south-westerly winds acting over areas 1, 2 and 3. At the same time, a band of surge elevation spread across the North Sea from the north of Scotland to Southern Norway and there was a lowering

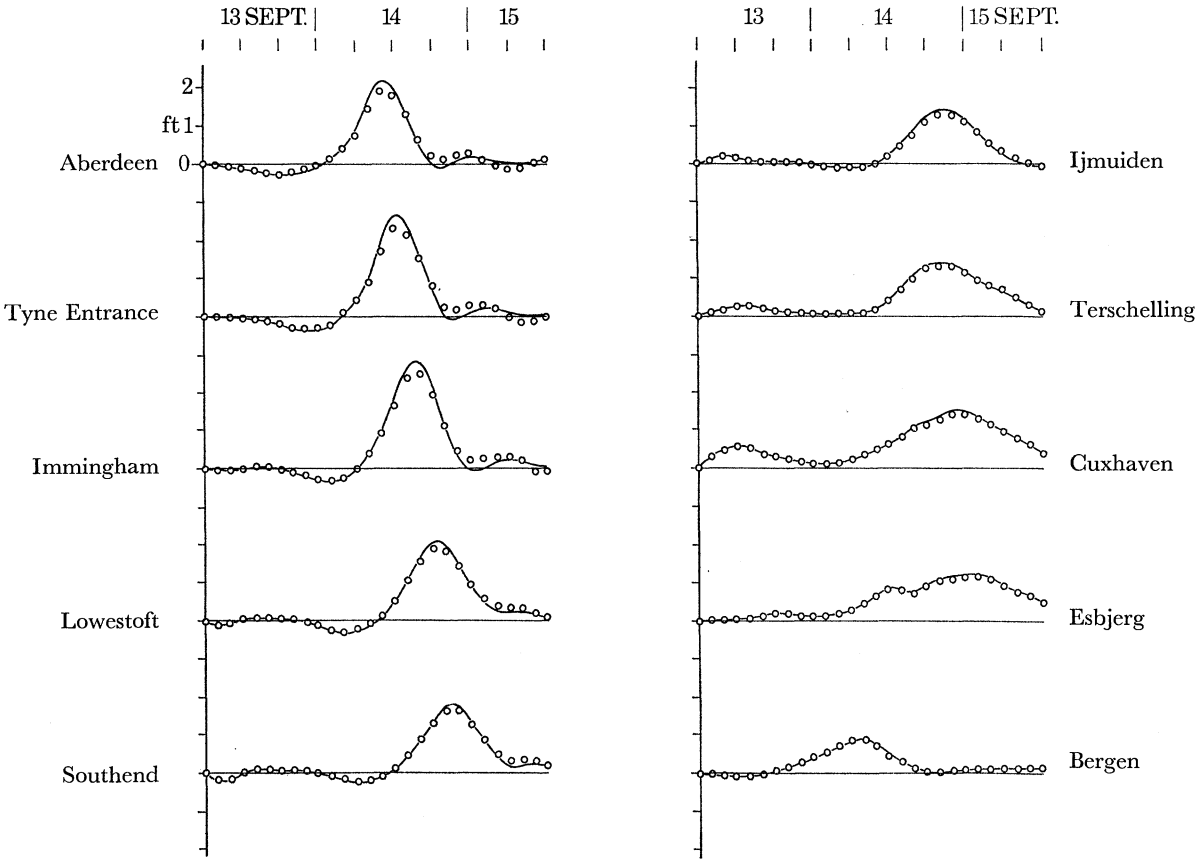

FIGURE 15. Storm surge of 13 to 15 September 1956; ——, wind surge from model 2; ○, wind surge from model 3.

of levels off the east coast of the British Isles—evidently caused by transport of water northwards under the influence of the wind fields acting over the northern areas. During the first 6 h of 14 September the surge maximum moved around the north coast of Scotland entering the North Sea; simultaneously, the band of elevation between Scotland and Norway intensified. As a result, at 06.00 h on 14 September a wave extended across the entrance to the North Sea, its crest lying in roughly an east to west line with amplitude decreasing with distance from the Scottish coast. Subsequently, the wave travelled southwards, affecting sea levels at ports on the east coast of England as shown in figure 14. The southwards progression took place between 06.00 and 18.00 h: the appropriate maps of figure 16 suggest that there was an accompanying flow of water into the North Sea from the sea region lying off the west coast of Norway. On reaching the southern boundary of the North Sea, after 18.00 h, the wave lost its progressive character and produced a general rise in level which rotated counterclockwise around the

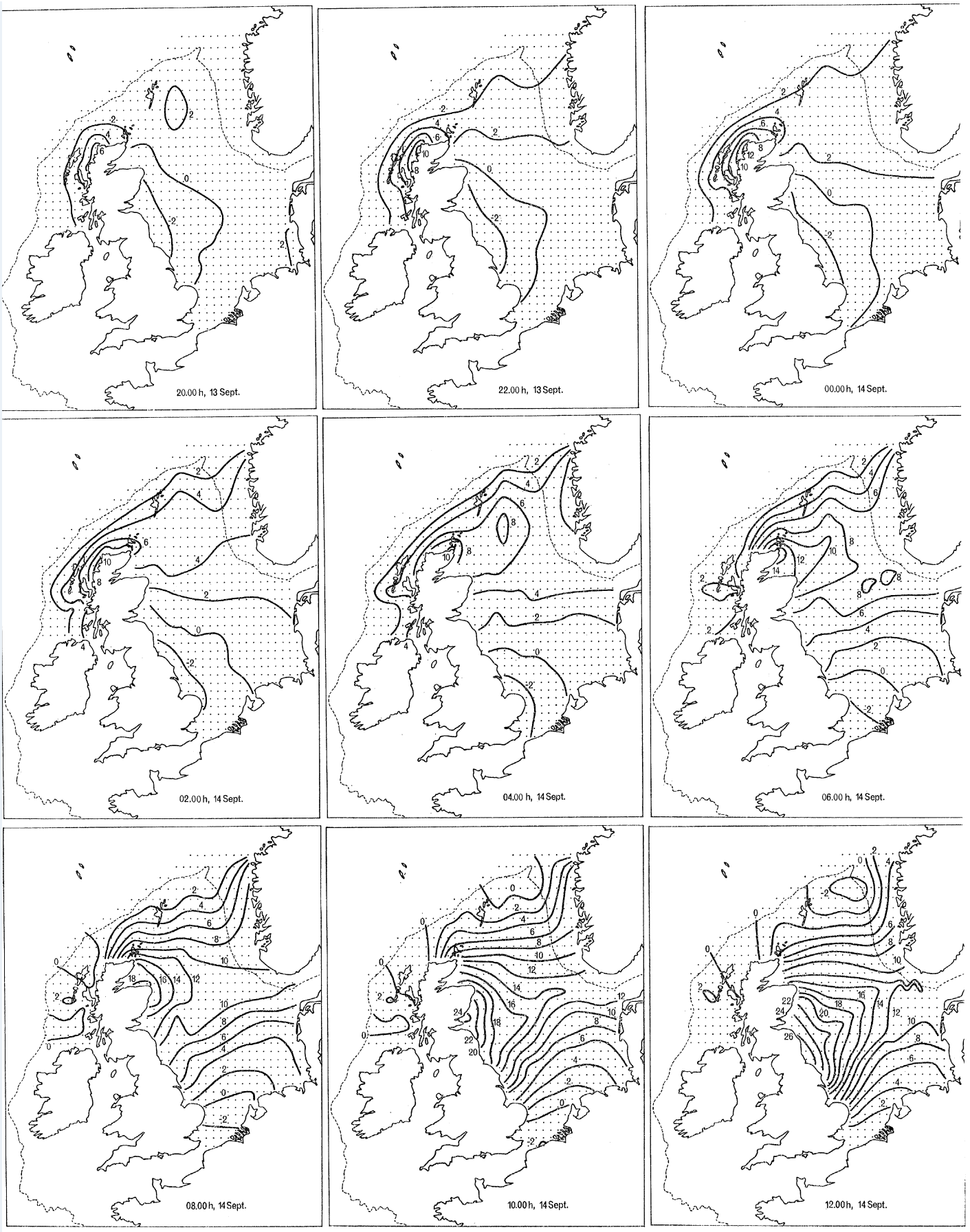

FIGURE 16. For legend see p. 124.

PHILOSOPHICAL TRANSACTIONS OF THE ROYAL SOCIETY A MATHEMATICAL, PHYSICAL & ENGINEERING SCIENCES

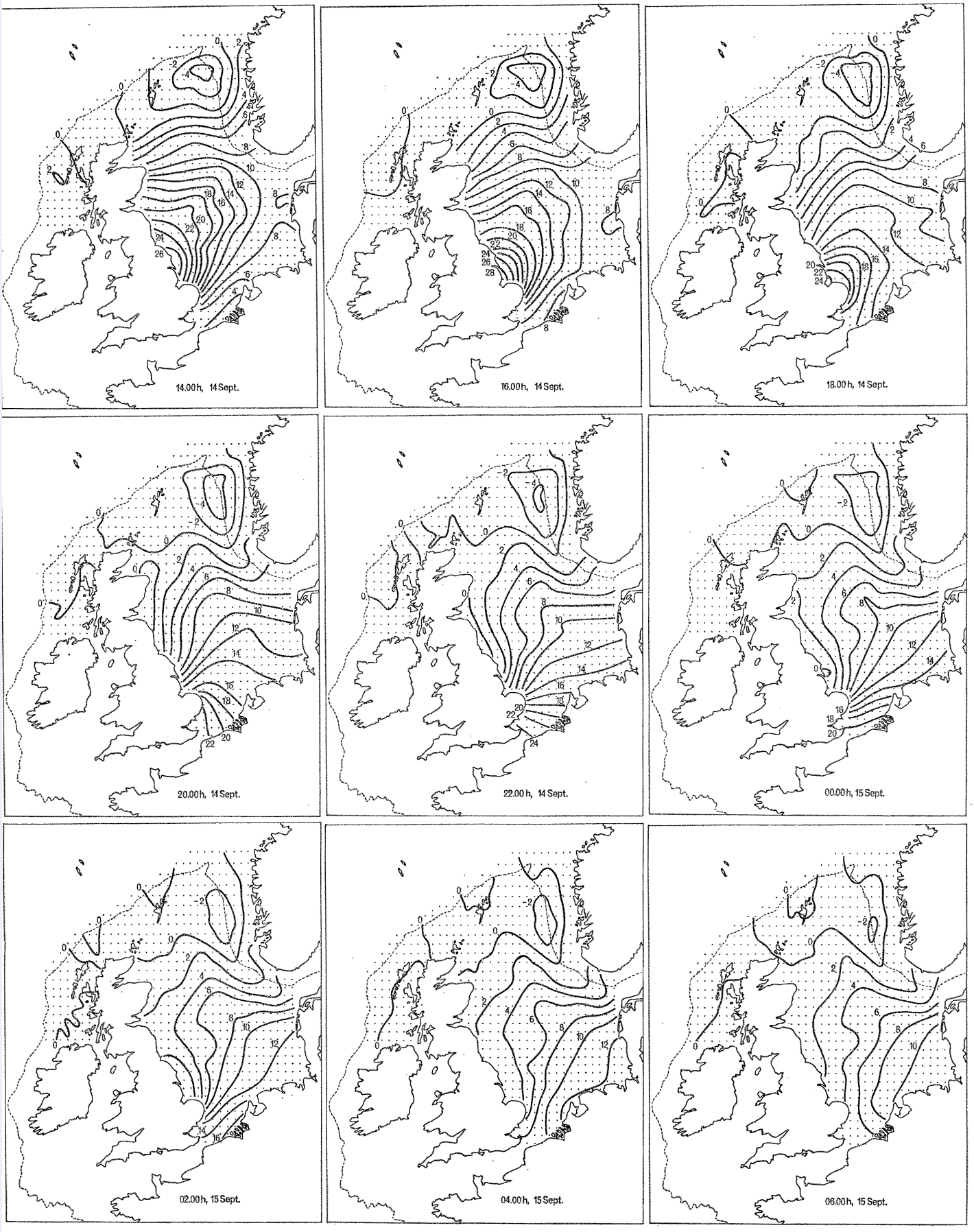

FIGURE 16. For legend see p. 124.

PHILOSOPHICAL TRANSACTIONS OF THE ROYAL SOCIETY A MATHEMATICAL, PHYSICAL & ENGINEERING SCIENCES

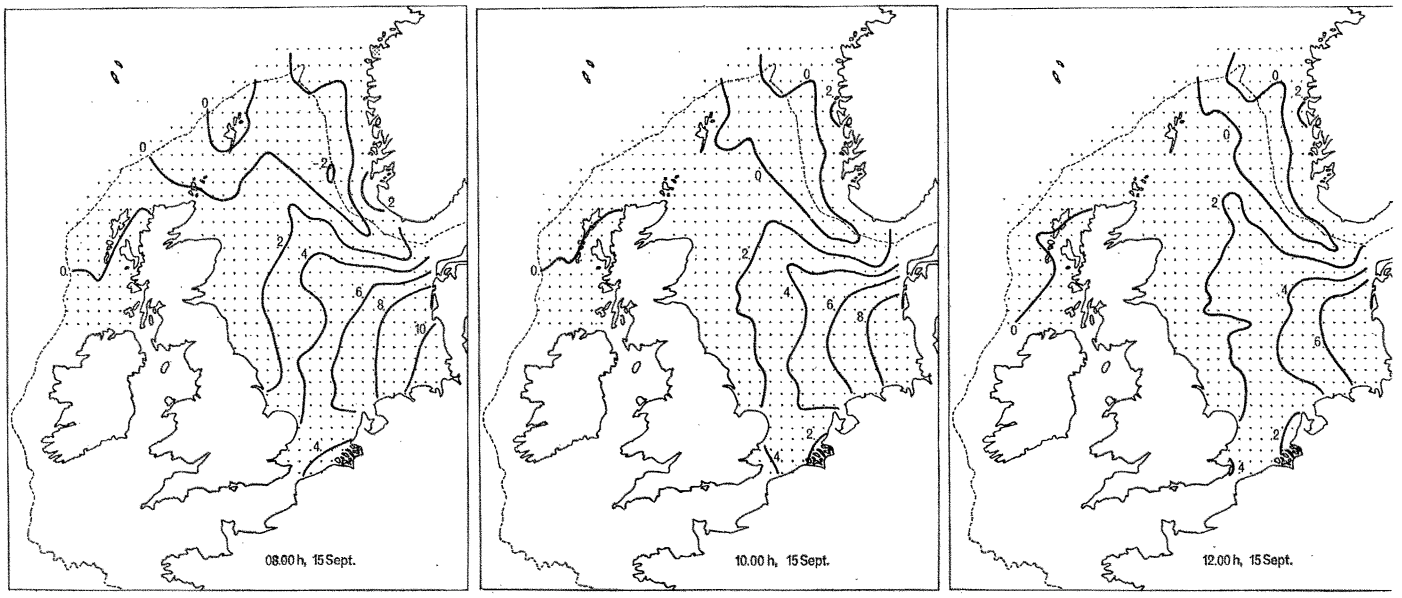

FIGURE 16. External surge of 13 to 15 September 1956; co-disturbance lines, showing elevations of sea level in units of 0.1 ft, calculated from model 1.

southern shores of the Sea, continually decreasing in amplitude. In all likelihood, the rotation of the disturbance was a geostrophic effect and the decrease in amplitude a consequence of high frictional dissipation in shallow water.

Thus, the development of the external surge consisted of the generation of the surge wave in northern waters followed by its free propagation within the North Sea. The characteristics of the propagation are illustrated in figure 17. Mapped out in this figure are lines along which maximum elevation occurred at the same time, also contours of maximum elevation. It is of considerable interest to find that these distributions are similar, respectively, to the co-tidal and co-range charts (given by the Wilhelmshaven Marine Laboratory in 1942) for each of the main diurnal tidal constituents K_1, O_1 and P_1 in the North Sea. There are no amphidromic points in the system for essentially it consists of a progressive wave motion from north to south only weakly reflected in the southern boundary. These results do not support the traditional idea of an external surge as being a localized disturbance in level which travels around the edges of the North Sea basin from Aberdeen to Bergen retaining its identity. Also, the assumption sometimes made in the past that this type of surge propagates in like manner to the principal semi-diurnal constituent, M_2, is not substantiated here.

Figure 18 throws some light on the generation of the surge wave on 13 and 14 September. Thus, figure 18*a* indicates that the winds over area 3 were very largely responsible for the disturbance. Considering the sequence of wind fields which acted over this area during the period, southerlies veering to southwesterlies and increasing in strength prevailed up to about 04.00 h on 14 September. Then followed, quite abruptly, a belt of very strong westerlies which veered towards the south as their strength decreased. The associated wind stress components (P, Q) over the area are plotted against time in figure 18*b* and it is noticeable that the southerly component P dropped to zero between 03.00 and 06.00 h as the westerly component Q attained its maximum. In the formation of the external surge it appears that water was driven to the north of the North Sea by the south and southwesterly winds, and that when the southerly component

of the wind diminished, the water held in the north was released to flow southwards into the North Sea off northeast Scotland. At the same time, water was being forced southwards, under the influence of the Earth's rotation, by the westerlies blowing at maximum strength. The combined effect, together with the propagation into the North Sea of surges generated by geostrophic deflexion against the northwest and north coasts of Scotland, produced the external surge. The timing of these various wind effects, to achieve superposition, was clearly of importance in the formation of the surge wave.

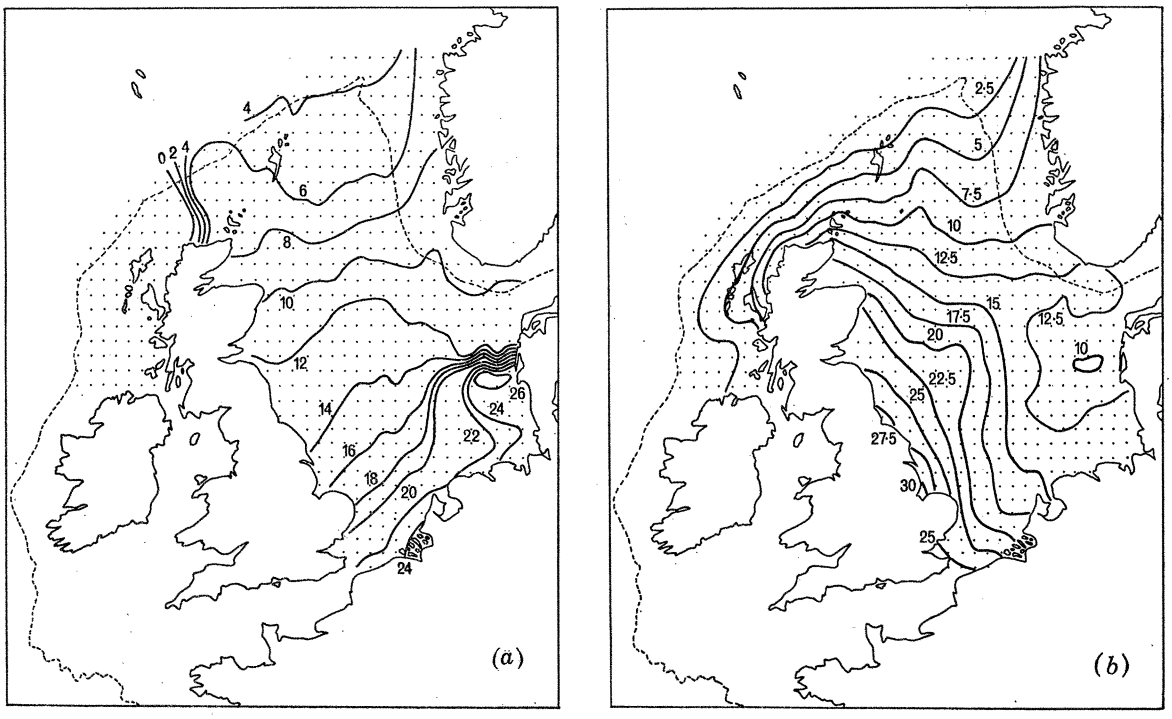

FIGURE 17. External surge of 13 to 15 September 1956: (*a*) lines along which maximum elevation occurred at the same time. The time associated with each line is shown in hours measured from 00.00 h on 14 September. (*b*) Contours of maximum elevation (in units of 0.1 ft).

Finally, it should be mentioned that the barometric surge in the North Sea, calculated from the statical law taking 1012 mb as mean atmospheric pressure, was relatively small during the period considered above: the general order of elevation values was -0.25 ft at the beginning of 14 September, changing slowly to -0.5 ft at noon on 15 September.

(*b*) *Internal surge*, 24 to 26 *February* 1958

The cause of this disturbance was a barometric depression which, on 25 February, moved up the length of the English Channel and subsequently passed into Northern France (figure 19). Strong northeasterly winds, backing to the north in the rear of the depression, were brought to bear on the waters of the southern North Sea, in particular on sea areas 11 and 13 shown in figure 11.

The residuals shown in figure 20 and the co-disturbance lines of figure 21 indicate that the winds piled water up against the coast of eastern England, raising levels in the Thames Estuary by between about 3 and 4 ft. Along the continental coast, especially in the German Bight, sea

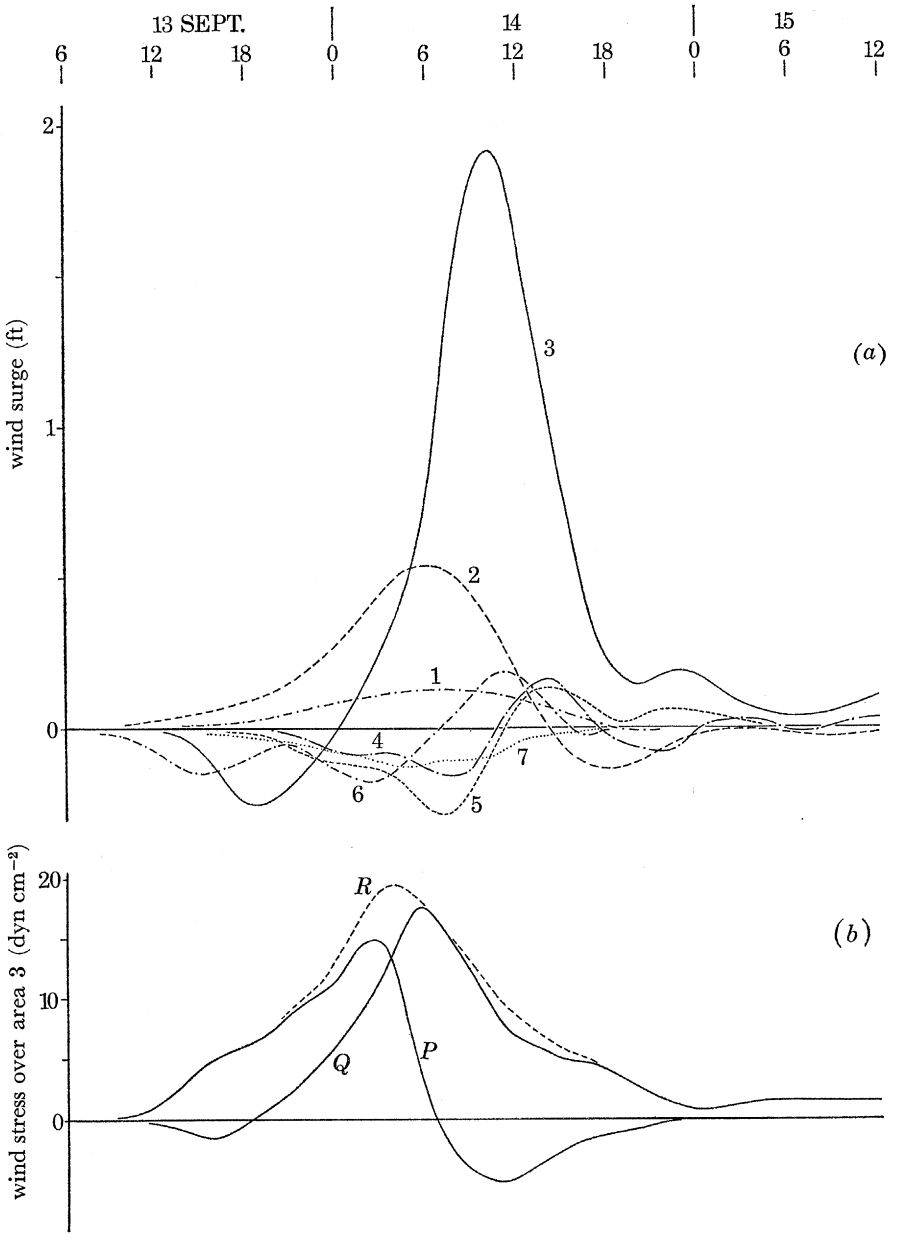

FIGURE 18. External surge, 13 to 15 September 1956: (*a*) contributions to the total calculated wind surge at Aberdeen originating from the various subareas of the North Sea. (*b*) The southerly and westerly components of wind stress (*P*, *Q*) over area 3, and their resultant *R*.

levels fell as water was driven across the North Sea towards the English shore line. Figure 22 confirms that the main surge-generating winds were those which acted over areas 11 and 13. The barometric surge (from the statical law) reached a maximum of approximately 0.9 ft in the extreme south of the North Sea as the centre of the depression passed over the area between 06.00 and 08.00 h on 25 February. All in all, the disturbance was truly 'internal' to the North Sea for there was very little surge effect in the northern sea regions.

Figure 20 shows that, on the whole, satisfactory agreement was obtained between calculated and observed surge levels. The actual surge at Southend was marked by large oscillations, of

semi-diurnal character, which clearly do not appear in the computed curves. The oscillations continued for some time after the surge had subsided: generally, peaks occurred on the rising tide and troughs on the falling tide. It seems probable that these fluctuations were associated with some nonlinear tide-surge interaction of the type described by Rossiter (1961); arguing in this way, the linearity of the hydrodynamical equations explains the absence of the phenomena in the numerical results. The rather large negative surges recorded at Esbjerg and Cuxhaven were

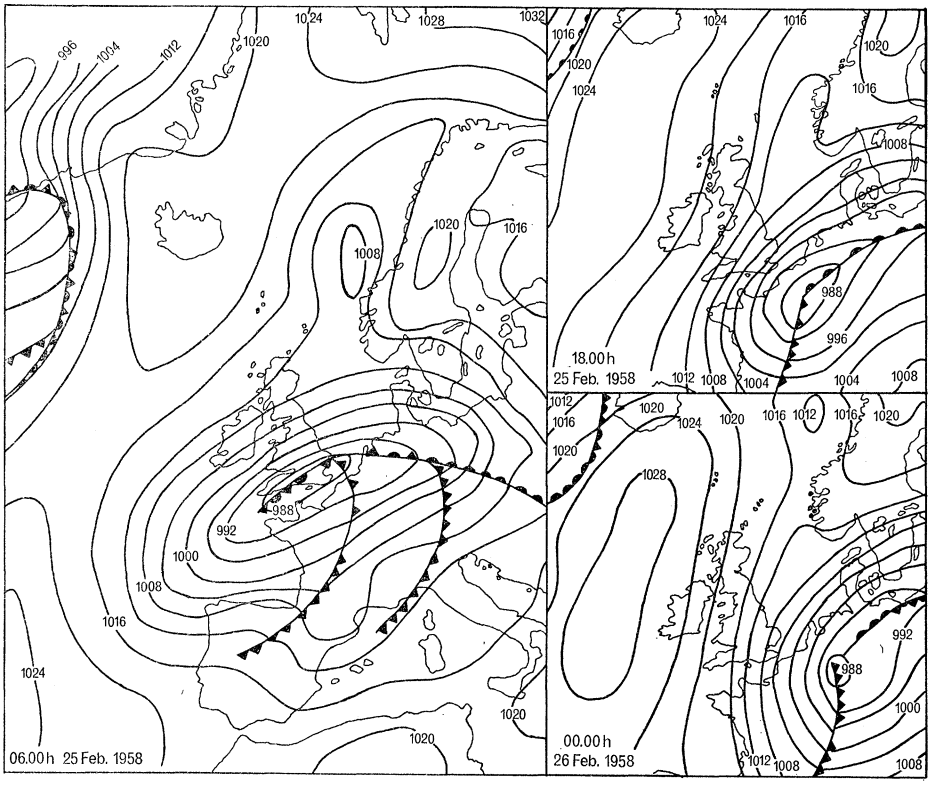

FIGURE 19. Weather charts for the storm surge of 24 to 26 February 1958.

not completely reproduced by the sea-model calculations, but one may suppose that this was due to the inability of the numerical models to take proper account of the lowerings of sea level produced by local off-shore winds blowing over extensive stretches of shallow coastal water.

The results obtained in this surge case from models 1 and 2, respectively, indicate that flow through the Dover Strait significantly lowered surge levels in the Southern Bight. Figure 20 shows that the lowering at Southend amounted to about 1 ft during and following the surge maximum. At Ijmuiden, the effect almost eliminated the positive surge on 26 February which originated from a counterclockwise rotation of elevation in the Bight—clearly demonstrated in figure 21 by the changing inclination of the co-disturbance lines. Output from model 2 gave a current surge through the Strait, directed out of the North Sea, with a maximum of 1.8 ft/s at 21.00 h on 25 February. The residual flow through the Strait was estimated using observations of the difference in electric potential on opposite sides of the English Channel as measured on the telephone cable running from St Margaret's Bay to Sangatte (see, for example, Bowden 1956).

The estimates showed that, between 18.00 h on 25 February and 06.00 h on 26 February, the current fluctuated between 1.5 and 2.7 ft/s, a variation in fair agreement with the maximum current derived from the numerical model calculations.

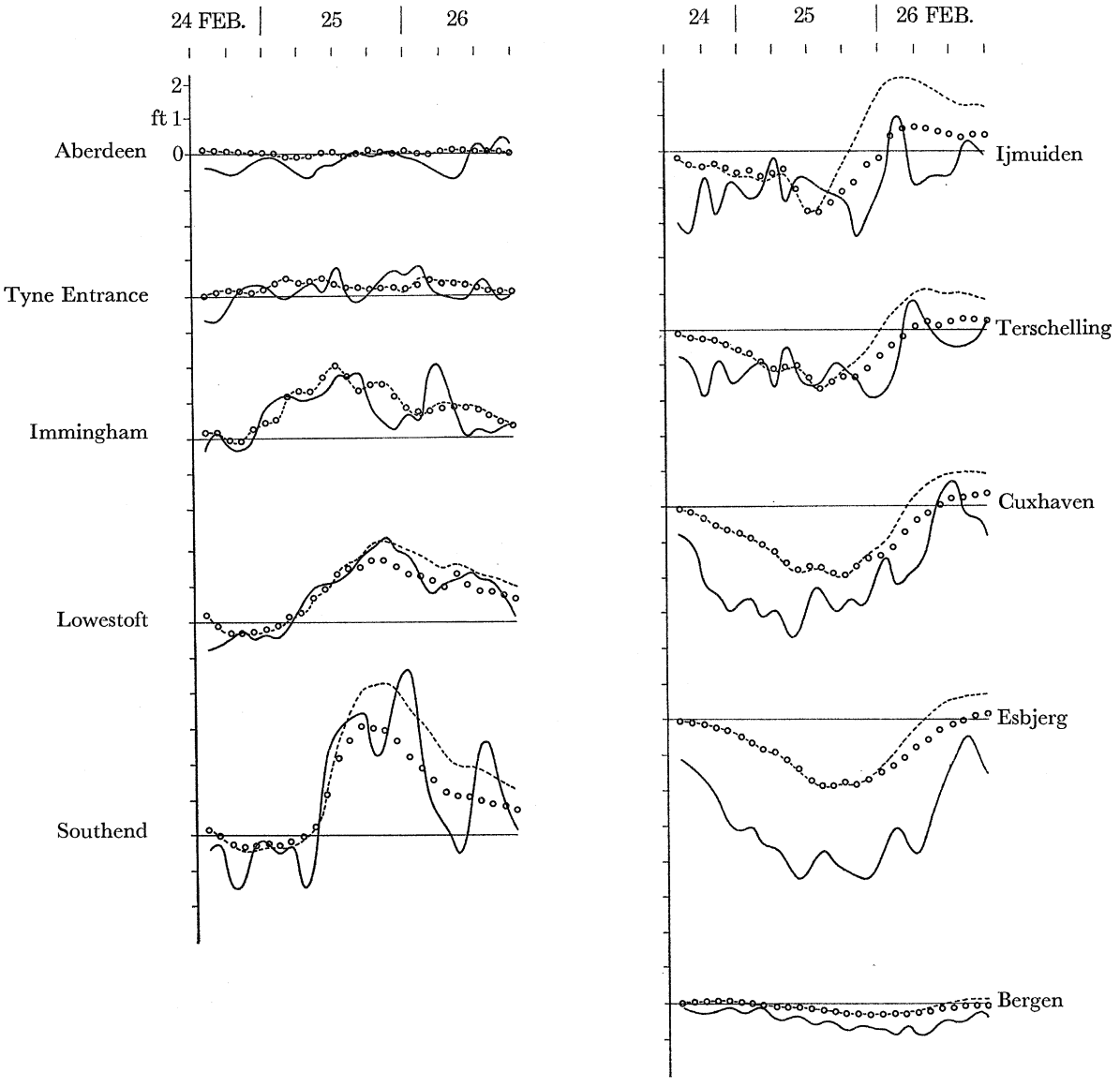

FIGURE 20. Storm surge of 24 to 26 February 1958; ——, residuals after removal of the barometric surge; ------, wind surge from model 1; ○, wind surge from model 2.

(*c*) *The 'Hamburg' surge*, 15 *to* 17 *February* 1962

This case may be regarded as representing the class of 'major' North Sea surges. The weather charts of figure 23 show that a large deep depression approached the west coast of Norway from the direction of Iceland and then passed southeastwards over Scandinavia into the Baltic. Gale force westerly to northwesterly winds, associated with the depression, extended over most parts of the North Sea impelling water towards its southern and southeastern coasts. As a result, large

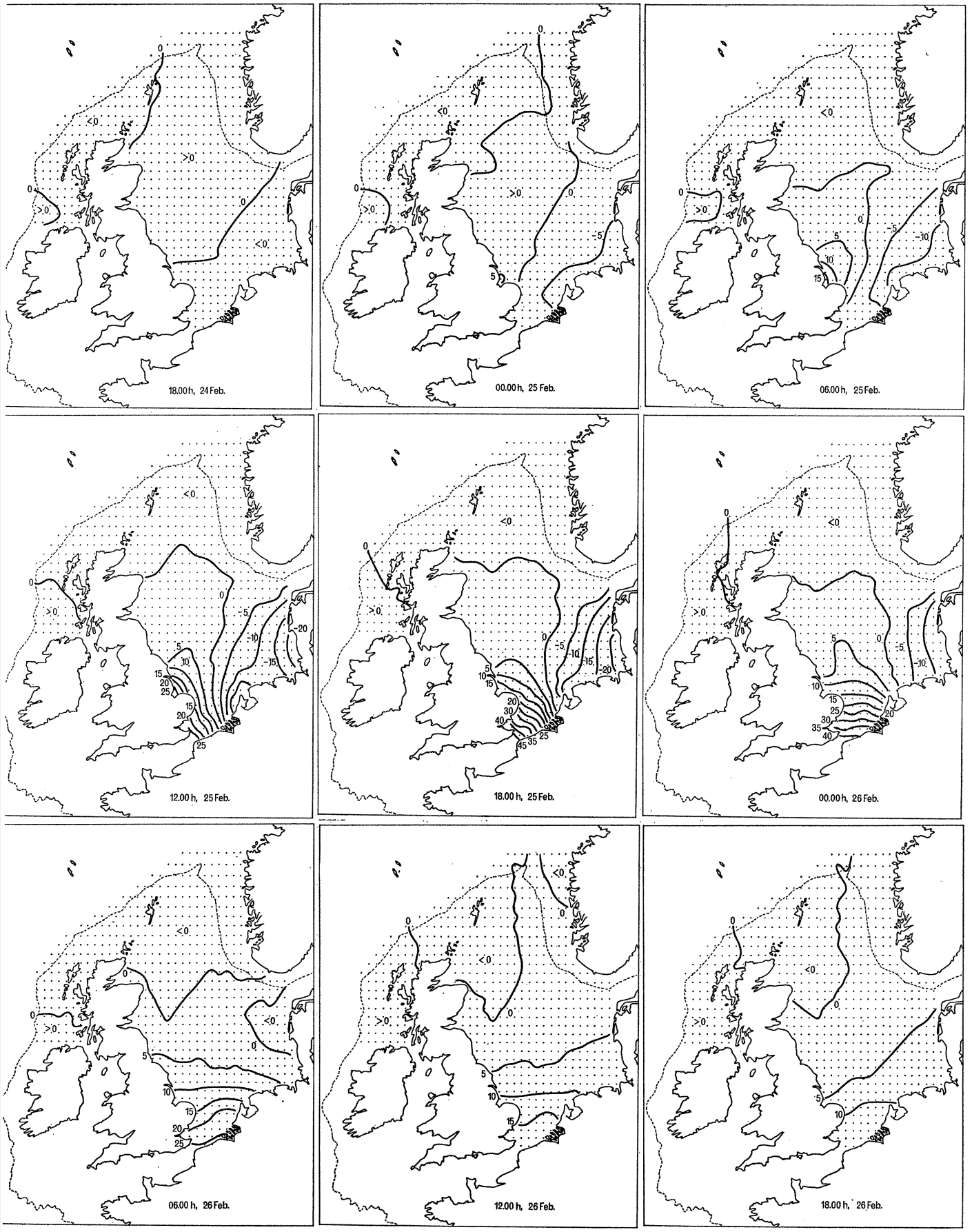

FIGURE 21. Surge in the south of the North Sea, 24 to 26 February 1958: co-disturbance lines, showing elevations of sea level in units of 0.1 ft, calculated from model 1.

PHILOSOPHICAL TRANSACTIONS OF THE ROYAL SOCIETY A MATHEMATICAL, PHYSICAL & ENGINEERING SCIENCES

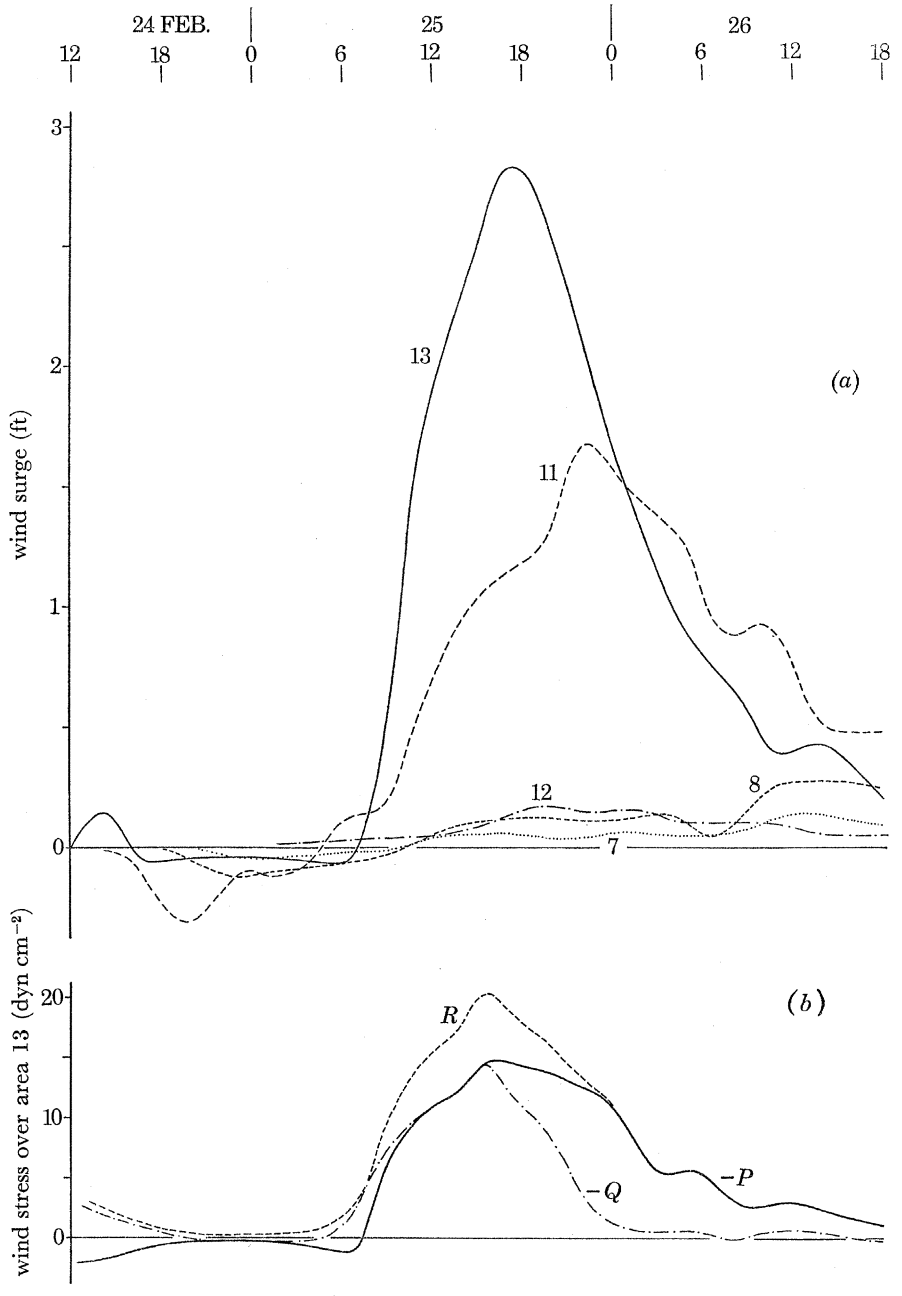

FIGURE 22. Surge in the south of the North Sea, 24 to 26 February 1958: (*a*) contributions to the total calculated wind surge at Southend originating from the various subareas of the North Sea. (*b*) The northerly and easterly components of wind stress ($-P$, $-Q$) over area 13, and their resultant R.

rises in sea level occurred along these boundaries, particularly so in the German Bight which was directly exposed to the most violent of the winds.

Figure 24 shows that the wind-induced elevation at Cuxhaven reached a maximum of over 11 ft at 00.00 h on 17 February. This rise in level was propagated into the Elbe Estuary, causing disastrous floods at Hamburg. Corresponding surge maxima of approximately 7 ft occurred at Southend, Ijmuiden, Terschelling and Esbjerg, respectively. The curves of figure 24 demonstrate

satisfactory agreement between surge heights derived from observations and those obtained using model 2. It is apparent that the results from model 1 considerably overestimated the elevations at Southend and Ijmuiden due to the assumption of a closed Strait of Dover. In reality, the residual current through the Strait (determined from measurements of difference in electric potential along the St Margaret's Bay–Sangatte telephone cable) was directed out of the North Sea and exceeded 2 ft/s for most of the period 20.00 h 16 February to 12.00 h 17 February; values of current derived from the runs with model 2 confirmed this fact. Manifestly, the surge

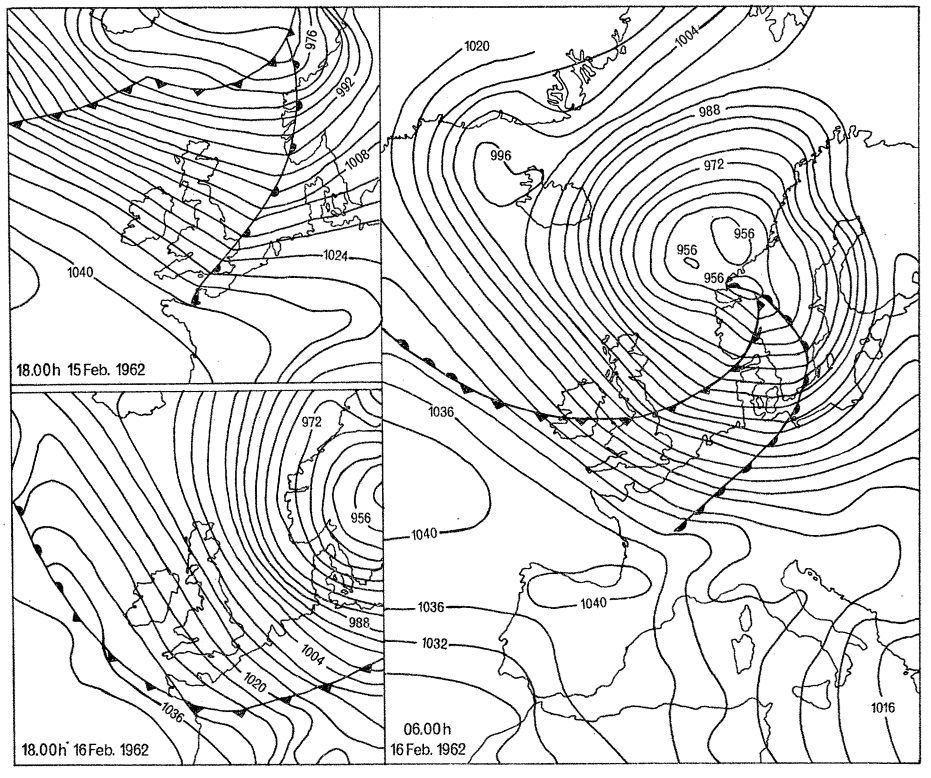

FIGURE 23. Weather charts for the storm surge of 15 to 17 February 1962.

at Southend was characterized by large oscillations of semi-diurnal type (as in the previous surge case) and that at Ijmuiden by smaller fluctuations of approximately quarter-diurnal period. One may argue again that these effects, not reproduced by the computations, may have originated from nonlinear processes, involving tide and surge, in the shallow coastal waters off each port.

The development, in space and time, of the wind-induced surge elevations is shown by the co-disturbance lines of figures 25 and 26. The patterns of figure 26 describe the build-up and subsequent decline of the main surge effect in the North Sea on 16 and 17 February. Changes in level induced prior to this, during the last half of 15 February and early on 16 February, are covered by figure 25. The latter figure indicates that part of the surge in the North Sea was due to 'external' disturbances, generated by the westerly winds against the northern coasts of Scotland, and then propagated into the western and southern regions of the Sea.

The lowering of atmospheric pressure over the North Sea during the storm was sufficiently great in the northeastern areas to produce statical elevations of the sea surface of up to 1 ft at

Esbjerg and 1.6 ft at Bergen. At the other ports considered in this paper, the corresponding elevations were generally much smaller—certainly not exceeding 0.7 ft, the peak value at both Cuxhaven and Aberdeen.

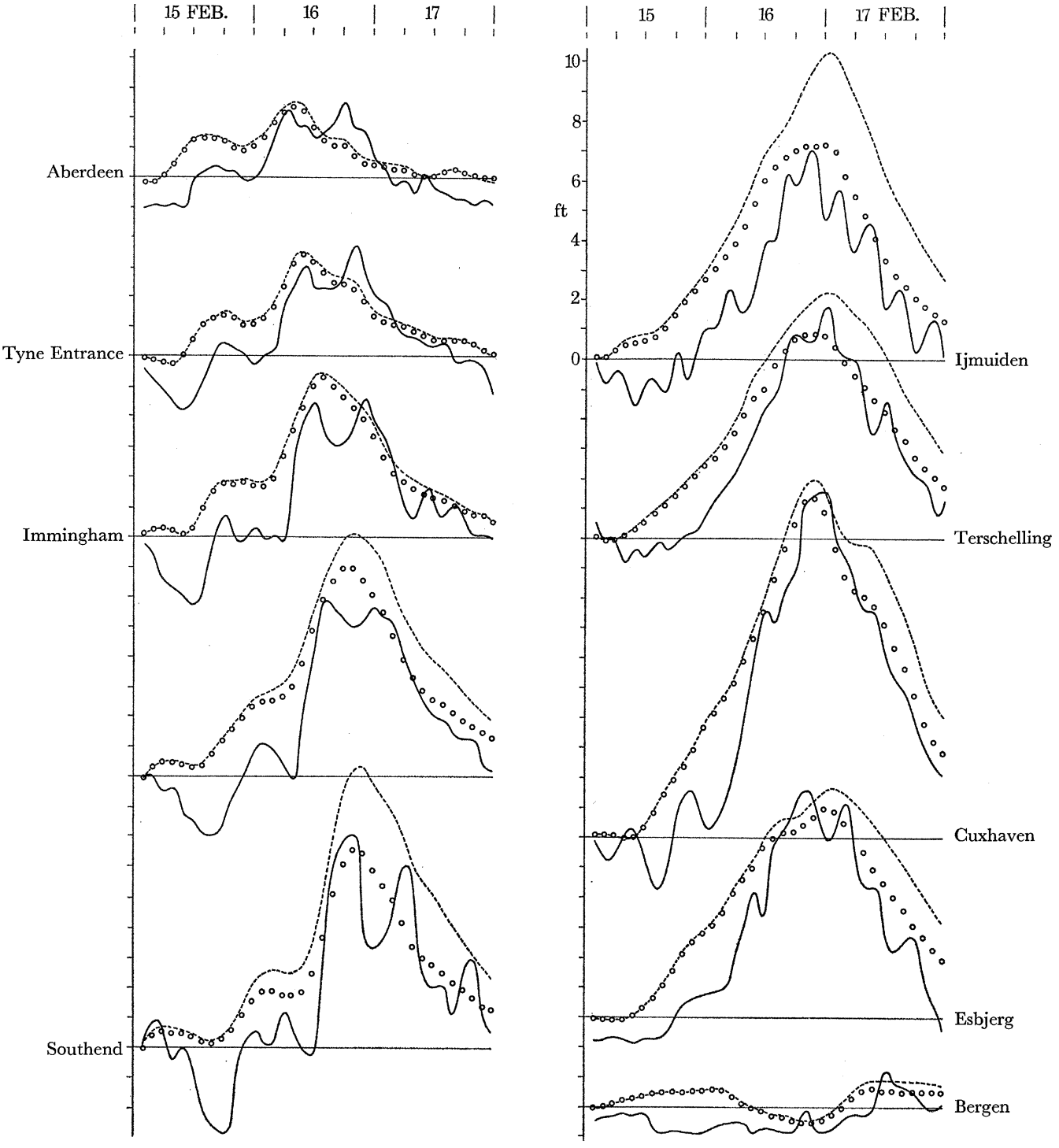

FIGURE 24. Storm surge of 15 to 17 February 1962; ——, residuals after removal of the barometric surge; ------, wind surge from model 1; ○, wind surge from model 2.

PHILOSOPHICAL TRANSACTIONS OF THE ROYAL SOCIETY A MATHEMATICAL, PHYSICAL & ENGINEERING SCIENCES

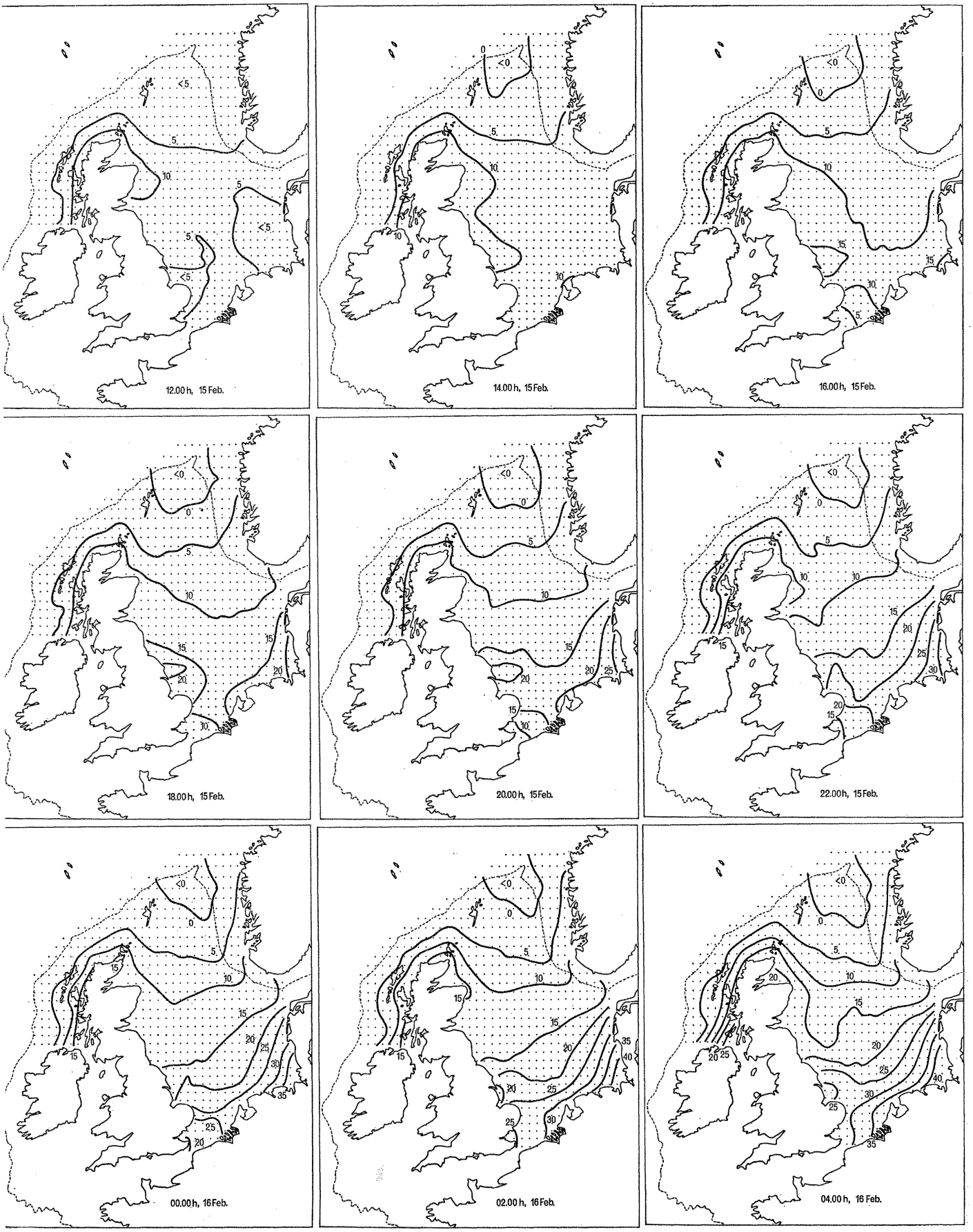

FIGURE 25. The 'Hamburg' surge of 15 to 17 February 1962: co-disturbance lines covering the period 12.00 h 15 February to 04.00 h 16 February, showing elevations of sea level in units of 0.1 ft, calculated from model 1.

PHILOSOPHICAL TRANSACTIONS OF THE ROYAL SOCIETY A MATHEMATICAL, PHYSICAL & ENGINEERING SCIENCES

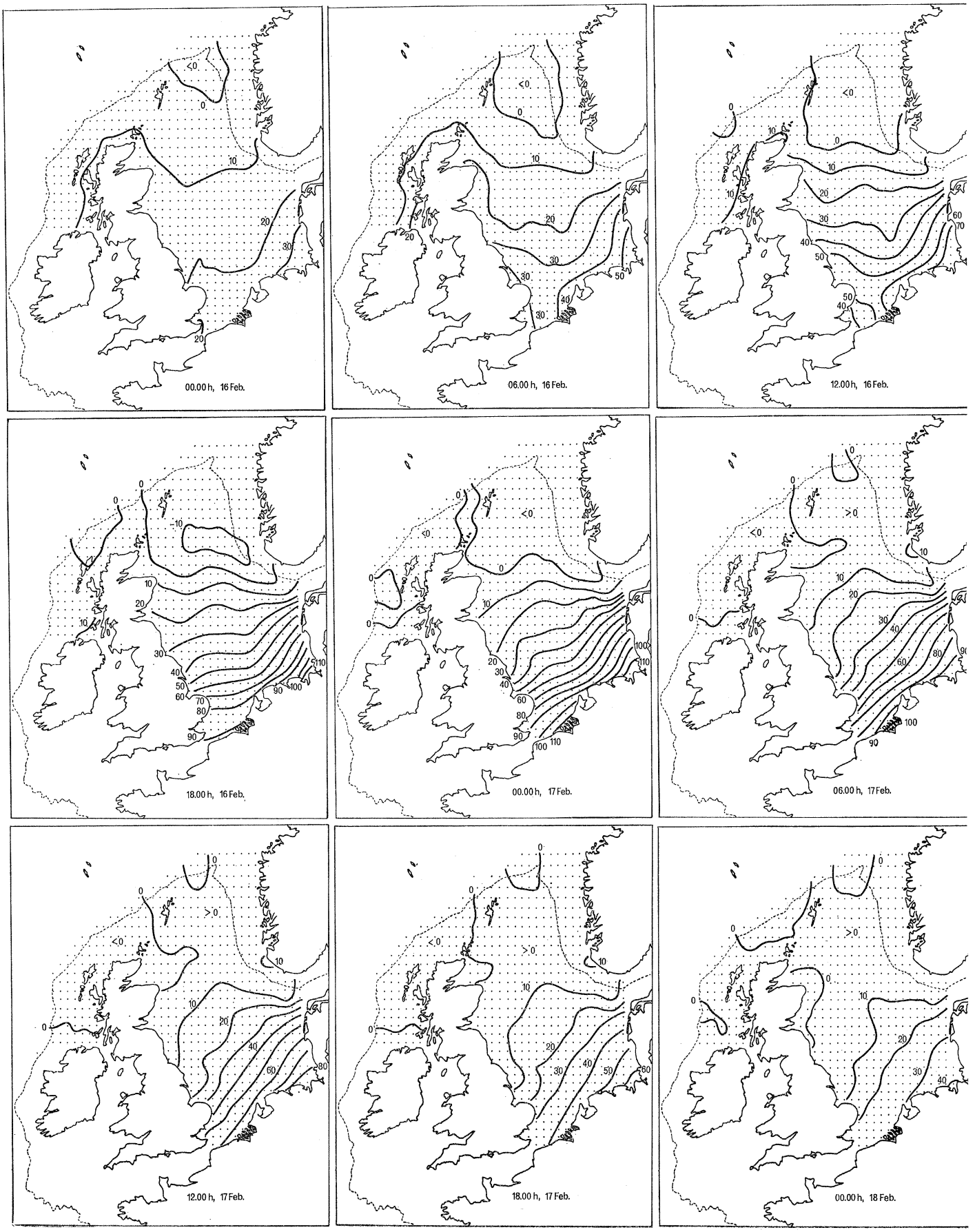

FIGURE 26. The 'Hamburg' surge of 15 to 17 February 1962: co-disturbance lines covering the period 00.00 h 16 February to 00.00 h 18 February, showing elevations of sea level in units of 0.1 ft, calculated from model 1.

PHILOSOPHICAL TRANSACTIONS OF THE ROYAL SOCIETY A MATHEMATICAL, PHYSICAL & ENGINEERING SCIENCES

10. Concluding remarks

A numerical sea model has been formulated in general terms, allowing representation of a wide range of sea basins of different depth and boundary configurations. In this approach, a model basin is constructed out of a number of basic elements or 'building bricks', covering various contingencies with respect to coastal boundary form, position, and orientation. A finite-difference scheme involving forward and backward differences in time, and central differences in space, has been used. Chosen initially for its simplicity and ease of application, the scheme is basically the one employed by Lauwerier (1962), here extended by expressing more carefully the conditions at a coastal boundary point: the equation of motion perpendicular to the boundary at such a point, previously ignored, is now taken into consideration. Applying the general theoretical structure, three models of successively increasing size have been set up for the purpose of computing storm surges in the North Sea. These determine the wind surge, which, in the North Sea, generally predominates over the barometric surge; the latter is estimated using the statical law.

Computations have been carried out for three periods covering, respectively, different types of North Sea surge. For each period, comparisons have been made between computed and observed surge profiles at a number of ports distributed around the shores of the North Sea. The results show that the sea-model calculations reproduced to a good first approximation the surge heights derived from sea-level records. Some of the discrepancies between the computed and observed values appear to have been due to the incomplete representation, in the models, of actual conditions in coastal waters—in particular, the approximate nature of the assumed marginal depth distributions and coastline configurations, along with the neglect of nonlinear effects. Other differences may have arisen because of the generally recognized uncertainties concerning the estimation of wind stress over the sea surface and the form and value of bottom friction. It is apparent from the results, computed with and without a barrier across the Dover Strait, that flow out of the North Sea into the English Channel produced significant lowerings of surge level in the Southern Bight. On the basis of computed elevations, patterns of co-disturbance lines have been drawn at regular intervals to show the changing spatial distribution of surge height during each of the periods considered.

A special study has been made of an external surge, since the origin and mode of propagation of such phenomena is a research topic of considerable interest. It has been found that the external wave was, for the most part, generated by wind action over the shelf waters lying in latitudes to the north of Scotland. Once formed in this region by a fairly complex but comprehensible sequence of events, the wave travelled southwards in the North Sea, exhibiting features similar to those of the diurnal tide. Weak reflexion at the southern boundary was responsible for the essential 'progressive wave' character of the motion, from north to south.

In addition to its immediate achievements, the present work has laid foundations for further research. It is envisaged that future investigations will deal with the extension and modification of the existing large model and its incorporation into an operational scheme of surge prediction. In the latter respect, a continuing practical aim is to develop a surge-forecasting system for ports on the east coast of England: the results so far obtained indicate that a satisfactory start has been made towards this goal.

Concerning possible extensions and modifications, finite-difference grids of finer mesh are required to represent more adequately the hydrography and motion in the coastal sea areas. Such grids, covering the coastal regions only, would connect with the coarser grid of the overall

PHILOSOPHICAL TRANSACTIONS OF THE ROYAL SOCIETY A MATHEMATICAL, PHYSICAL & ENGINEERING SCIENCES

sea model. The connexions could take the form of a 'patching' together of the different mesh systems along their common boundaries (Jelesnianski 1965). Alternatively, input of elevation along the sea boundaries of the subsidiary coastal models might be taken from values calculated with the larger parent model (Miyazaki 1965). It would be important to include nonlinear effects in the fine-mesh calculations (covering, as they would, the shallow-water regions) and this would necessitate the combined reproduction of tides and storm surges in the computations. The ability to generate co-oscillating tides would, of course, depend on a knowledge of the tidal variations along bounding sections drawn across the open sea.

The lateral extension of the existing models beyond the edge of the continental shelf, to include substantial areas of the deep sea, is desirable in order to take account of meteorologically induced disturbances in the ocean and their effects in the shelf region. Work with models of this magnitude will become possible as computers grow in size, providing increased storage capacity and facilities for handling, recording and plotting the great volume of output data which could be expected. A more fundamental development, following on from the present analysis, would be the numerical solution of the basic three-dimensional hydrodynamical equations, involving the depth coordinate as an additional independent variable. Solutions would determine horizontal current as a function of depth, horizontal position and time, in addition to the varying distribution of sea-surface elevation. The approach would replace the present use of vertically-integrated forms and would enable bottom friction to be formulated in terms of bottom current, as well as yielding details of the current structure. Values of eddy viscosity would, however, be required throughout the sea.

There is a need for research into the meteorological problem of determining values of wind velocity and pressure for sea-model input. The rather long and laborious methods of evaluation based on the analysis of weather charts, currently employed, should eventually give way to the use of output from a numerical weather-prediction model. From such output, one could expect to derive, rapidly and systematically, both the wind and pressure at individual sea-model grid points, at short regular intervals of time. This would open up the possibility of placing storm-surge prediction on an operational basis along with weather forecasting itself. Also, the easy availability, in numerical form, of the detailed distribution of atmospheric pressure over the sea surface, would facilitate the estimation of pressure gradient for inclusion as an atmospheric forcing term in the hydrodynamical equations. The dynamic effects in the sea of variations in atmospheric pressure, ignored here, would then be represented in the sea-model results.

In addition to the approach of the present paper, other methods are being employed in the study and theoretical reproduction of North Sea surges. Mention should be made of the electronic analogue model developed by Ishiguro (1962, 1966), and the response function analysis of Cartwright (1968). A critical comparison of results obtained from the different methods will be of interest when the potentialities of each have been explored further. With regard to related work, it should be noted that purely analytical investigations on the propagation of tidal waves, such as those carried out by Crease (1956, 1958) and Buchwald (1968), can yield useful insights into the mechanics of sea motion not readily perceived from numerical solutions. Clearly, it is important that the analytical and numerical approaches, which are in many ways complementary, should be pursued in close relation to each other.

I am grateful to Dr J. R. Rossiter for his support, and to members of the staff of the Tidal Institute for their assistance, during the various stages of this work. Also, I am indebted to

PHILOSOPHICAL TRANSACTIONS OF THE ROYAL SOCIETY A MATHEMATICAL, PHYSICAL & ENGINEERING SCIENCES

Mr F. H. Bushby and Mr J. F. Keers of the Meteorological Office for their cooperation in providing wind data.

References

Banks, J. E. 1967 A numerical model to study tides and surges in a river–shallow sea combination, M.Sc. Thesis, University of Liverpool.

Bowden, K. F. 1953 *Proc. Roy. Soc.* A **219**, 426–446.

Bowden, K. F. 1956 *Phil. Trans.* A **248**, 517–551.

Buchwald, V. T. 1968 *J. Fluid Mech.* **31**, 193–205.

Cartwright, D. E. 1968 *Phil. Trans.* A **263**, 1–55.

Charnock, H. & Crease, J. 1957 *Sci. Progr., Lond.* **45**, 494–511.

Corkan, R. H. 1948 *Storm surges in the North Sea*, vols I and II. U.S. hydrogr. Off., Misc. 15072, Washington, D.C.

Crease, J. 1956 *J. Fluid Mech.* **1**, 86–96.

Crease, J. 1958 *J. Fluid Mech.* **4**, 306–320.

Dantzig, D. van & Lauwerier, H. A. 1960*a* *Proc. K. ned. Akad. Wet.* A **63**, 170–180.

Dantzig, D. van & Lauwerier, H. A. 1960*b* *Proc. K. ned. Akad. Wet.* A **63**, 339–354.

Findlater, J. *et al.* 1966 *Scient. Pap. met. Off., Lond.* no. 23.

Fischer, G. 1959 *Tellus* **11**, 60–76.

Fischer, G. 1965 *Mon. Weath. Rev. U.S. Dep. Agric.* **93**, 110–111.

Groen, P. & Groves, G. W. 1962 *The sea*, vol. I, 764–801. New York and London: Interscience Publishers.

Hansen, W. 1956 *Tellus* **8**, 287–300.

Hansen, W. 1962 *Proc. Symp. math.-hydro. methods of phys. oceanography* (ed. W. Hansen), pp. 25–34. Hamburg University.

Hansen, W. 1966 *Mitt. Inst. Meereskunde Univ. Hamburg*, no. 5.

Harris, D. L. & Jelesnianski, C. P. 1964 *Mon. Weath. Rev. U.S. Dep. Agric.* **92**, 409–422.

Harris, D. L. & Jelesnianski, C. P. 1965 *Mon. Weath. Rev. U.S. Dep. Agric.* **93**, 111.

Heaps, N. S. 1965 *Phil. Trans.* A **257**, 351–383.

Heaps, N. S. & Ramsbottom, A. E. 1966 *Phil. Trans.* A **259**, 391–430.

Heaps, N. S. 1967 *Oceanogr. Mar. Biol. Ann. Rev.* **5**, 11–47.

Ishiguro, S. 1962 *Proc. Symp. math.-hydro. methods of phys. oceanography* (ed. W. Hansen), pp. 265–269. Hamburg University.

Ishiguro, S. 1966 *Nat. Inst. Oceanogr. Rep.* no. 4.

Jelesnianski, C. P. 1965 *Mon. Weath. Rev. U.S. Dep. Agric.* **93**, 343–358.

Jelesnianski, C. P. 1966 *Mon. Weath. Rev. U.S. Dep. Agric.* **94**, 379–394.

Jensen, H. E. & Weywadt, S. 1966 *Tech. Rep. Nato Subcttee on Oceanogr. Res.* no. 28. Technical University of Denmark, Copenhagen.

Laska, M. 1966 *Arch. Hydrot.* **13**, 335–366.

Lauwerier, H. A. 1960*a* *Proc. K. ned. Akad. Wet.* A **63**, 266–278.

Lauwerier, H. A. 1960*b* *Proc. K. ned. Akad. Wet.* A **63**, 279–290.

Lauwerier, H. A. 1960*c* *Proc. K. ned. Akad. Wet.* A **63**, 423–438.

Lauwerier, H. A. 1961*a* *Proc. K. ned. Akad. Wet.* A **64**, 104–122.

Lauwerier, H. A. 1961*b* *Proc. K. ned. Akad. Wet.* A **64**, 418–431.

Lauwerier, H. A. 1962 *Proc. Symp. math.-hydro. methods of phys. oceanography* (ed. W. Hansen), pp. 13–24. Hamburg University.

Lauwerier, H. A. & Damsté, B. R. 1963 *Proc. K. ned. Akad. Wet.* A **66**, 167–184.

Leendertse, J. J. 1967 *Memor. Rand Corp., Santa Monica, Calif.* RM-5294-PR.

Miyazaki, M. 1965 *Oceanogrl Mag.* **17**, 109–140.

Miyazaki, M., Ueno, T. & Unoki, S. 1961 *Oceanogrl Mag.* **13**, 51–75.

Miyazaki, M., Ueno, T. & Unoki, S. 1962 *Oceanogrl Mag.* **13**, 103–117.

Platzman, G. W. 1958 *Geophysica* **6**, 407–438.

Platzman, G. W. 1963 *Met. Monogr.* **4**, no. 26.

Platzman, G. W. 1965 *Mon. Weath. Rev. U.S. Dep. Agric.* **93**, 275–281.

Proudman, J. 1954 *Mon. Not. R. astr. Soc. geophys. Suppl.* **7**, 44–48.

Richtmyer, R. D. 1957 *Difference methods for initial-value problems*. New York and London: Interscience Publishers.

Rossiter, J. R. 1959 *Q. Jl R. met. Soc.* **85**, 262–277.

Rossiter, J. R. 1961 *Geophys. J. R. astr. Soc.* **6**, 29–53.

Sielecki, A. 1968 *Mon. Weath. Rev. U.S. Dep. Agric*, **96**, 150–156.

Ueno, T. 1964 *Oceanogrl Mag.* **16**, 53–124.

Uusitalo, S. 1960 *Tellus* **12**, 427–435.

Veltkamp, G. W. 1954 *Rapp. Afd. toegep. Wisk. math. Cent.* TW 24.

Weenink, M. P. H. 1958 *Meded. Verh. K. ned. met. Inst.* **73**, 111 pp.

Welander, P. 1961 *Adv. Geophys.* **8**, 315–379. New York and London: Academic Press.

PHILOSOPHICAL TRANSACTIONS OF THE ROYAL SOCIETY A MATHEMATICAL, PHYSICAL & ENGINEERING SCIENCES